ON ULTRASONIC SIGNAL PROCESSING AND ITS APPLICATION TO TOMOGRAPHIC RECONSTRUCTION

by

KANDREGULA PRASAD

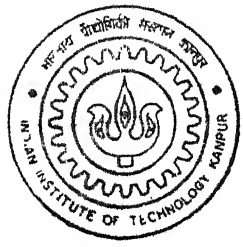

DEPARTMENT OF MECHANICAL ENGINEERING

Indian Institute of Technology, Kanpur

April, 2001

ON ULTRASONIC SIGNAL PROCESSING AND ITS APPLICATION TO TOMOGRAPHIC RECONSTRUCTION

A Thesis Submitted

in Partial Fulfillment of the Requirements

for the Degree of

MASTER OF TECHNOLOGY

by

KANDREGULA PRASAD

to the

DEPARTMENT OF MECHANICAL ENGINEERING

INDIAN INSTITUTE OF TECHNOLOGY KANPUR

APRIL, 2001

CERTIFICATE

It is certified that the work contained in the thesis entitled **ON ULTRASONIC SIGNAL PROCESSING AND ITS APPLICATION TO TOMOGRAPHIC RECONSTRUCTION** by *Kandregula Prasad* has been carried out under my supervision and that this work has not been submitted elsewhere for a degree.

N N Kishore 30/4/01

Dr. N. N. Kishore
(Professor)
Department of Mechanical Engineering,
Indian Institute of Technology, Kanpur.

April, 2001

DEDICATED

TO

MY BELOVED PARENTS

ACKNOWLEDGEMENTS

I wish to express my profound gratitude and indebtedness towards my thesis supervisor Dr. N.N. Kishore for his inspiring guidance, invaluable suggestions and constant encouragement.

I wish to extremely thankful to Mr. S. K. Rathore for his valuable suggestions and constant encouragement towards completion of my Thesis.

I wish to express my thanks to Dr. V. Raghuram for his suggestions and encouragements. I appreciate and extend my thanks to my lab mates Dr. A. K. Agrawal, Shashi bhushan, Samuel, Bnrao, Dali raju, Sarin and Trivedi.

I would like to thank all of my friends Swaroop, Kovvila, PLN, Ganesh, Narendra, Ramesh, Lachi, KNS, Challa, Bhanu, Anil and Laxman for making my stay at IITK very enjoyable and memorable. I will cherish the moments forever.

I wish to record my special thanks to my uncle Mr. P. Ramana babu and my cousin for motivating me to pursue my M. Tech program. I wish to extend my thanks to my sisters and cousin. I am also very much thankful to my Uncle Mr. M. Apparao for his valuable help.

Indian Institute of Technology, Kanpur. Kandregula Prasad

April 2001

ABSTRACT

In Ultrasonic Non-destructive testing and Evaluation (NDE), the different features of ultrasonic waves, namely frequency, amplitude, time of flight etc. can be used for detection and sizing of internal defects. Ultrasonic Tomography (UT) is used to characterize a defect or in-homogeneity by Time of Flight (TOF) information. The accuracy of reconstruction depends on the correctness of TOF determination. The present work is on the use of signal processing techniques for TOF measurement and consequent image reconstruction. In practice, the ultrasonic beams in an elastic medium is generated by one probe (transmitter) and received through another probe (receiver). An Automated Ultrasonic Experimental Setup was used for data acquisition in an A-scan format. Discrete Wavelet Transform (DWT) was used for noise suppression from all the acquired signals, by using 'db5' mother wavelet. Samples were prepared using combinations of Perspex and Nylon as base materials and Epoxy resin and Aluminium as insert materials. When, a pulse wave is received through an interface, the signal has overlapped modes. The modes of these overlapped (i.e. multi-path) signals were separated by using least-squares method and cross correlation method. Criterion for selection of a mode was based on the number of reference signals available. Based on these results, an energy-based criterion has been proposed for the selection of desired mode from the separated modes. The Time of Flight of these modes have been used for tomographic reconstruction of a specimen having defect using a Multiplicative Algebraic Reconstruction Technique (MART) algorithm. The reconstructed images for 2-view and 4-view projections are presented and it has been shown that for reconstruction of true shape, 2-view projections are not sufficient. The effect of relaxation parameter (λ) on the reconstruction accuracy and convergence rate has also been studied.

CONTENTS

List of Figures

List of Tables

List Of Symbols

$f(t)$	Signal
t	Time
τ	Time-shift
ω, ν	Frequency
$F(\omega)$	Signal in frequency-domain
$w(t-\tau)$	Window function
a	Scaling parameter
b	Translation parameter
$F(\omega)$	Fourier Transform
$W_f(a,b)$	Wavelet Transform
$\psi(t)$	Mother wavelet function
$C(a,b)$	Wavelet coefficient
$s(t)$	Ultrasonic signal
$y(t)$	De-noised signal
$n(t)$	Noise
$S(t)$	De-noised multi path (overlapped) signal
$R(t)$	De-noised reference signal
A_i	Amplitude
N	Number of modes in multi path signal
e_i	Error
E	Total square error in Least squares method
$C_{RS}(\tau)$	Correlation of signal R and S as a function of time delay τ
M	Number of data points in the Signal
T	Total time range
s_p	Separated p^{th} mode from a multi path signal
EN	Energy
ptd	Post trigger delay

s^k	Slowness in the k^{th} pixel
w_{ij}	Weight (length of intercept) of the i^{th} ray in the j^{th} pixel
λ	Relaxation parameter

Chapter 1

INTRODUCTION

1.1 INTRODUCTION

Non-Destructive testing and Evaluation (NDE) techniques play a major role in quality assurance of structural members during manufacturing stage and operating life. Being one of the most commonly used Non-destructive Testing (NDT) methods, Ultrasonic Testing (UT) is fast developing in the recent years. The UT method uses ultrasonic waves for detection and sizing of internal defects of materials. In this, piezo-electric transducer (probe) generates ultrasonic waves, which propagate in the elastic medium and are detected either by the same or by a different transducer.

In general the transit time of the acoustic echo wave is used to measure the distance of a flaw/insertion from the probe and the amplitude of the reflected wave is used to size the flaw. In the *pulse echo* technique, a single probe is used to transmit and receive the signal. Another technique called *through transmission* employs two separate transducers (a transmitter and a receiver) to transmit and receive the wave. This technique requires access to both sides of the specimen, as the probes are placed on opposite sides of the specimen.

Ultrasonic signals can be displayed in A-scan, B-scan or C-scan formats. An A-scan indicates a variation of signal amplitude with time at a point. The familiar screen image is on A-scan presentation, which furnishes one-dimensional description of a given test point. In the case of B-scan, the displayed signal is a time versus linear position trace. In case of two-dimensional (area) scanning of test piece, the test results can be represented by means of a C-scan. This furnishes a top view of the scanned surface. C-scan systems are usually computer controlled and the image displayed is colour coded to facilitate interpretation. Ultrasonic systems displaying both B-scan and C-scan formats are called P-scan systems.

Wavelet analysis in ultrasonic nondestructive applications has been shown to be a useful tool for the interpretation and enhancement of ultrasonic data in the context of

nondestructive evaluation. The Wavelet Transform (WT) divides the signal into different frequencies/scales/levels in terms of basis functions obtained by compression/dilation and translation of mother wavelet. Compared to other time-frequency representations like short time Fourier transform and Wigner-ville transform, the wavelet transform provides spectral representation and temporal order of the signal components simultaneously. Another important property is that the signal reconstruction does not involve global averaging in time or frequency domains because of good localization of the wavelet coefficients in both domains.

In ultrasonic techniques, information on defect characterization requires more evolved techniques than classical methods. Modern non-destructive testing of materials has to provide the highest possible detection probability, the correct size and exact orientation of defects in the specimen. The simplest mechanical acoustical characterizations of materials deal with velocity measurements. Due to mode conversion of the solid-solid/ liquid-solid interface, two quasi waves coexist in the solid medium. The spatial and temporal separations of the two modes are limited in certain conditions.

The technique of Computerized Tomography (CT) has established itself as a leading tool in diagnostic radiology over past thirty years, and is being applied in the NDE of engineering structures in a variety of situations. Image reconstruction from projections is based either on transform methods or on series expansion methods. Series expansion methods are iterative.

This study is on the reconstruction of the samples with artificially implanted defects is carried out using Ultrasonic Computed Tomography (UCT). When a pulse wave is received through a region of in-homogeneity interface, the signal may have two or more overlapped modes. The accurate and correct TOF data estimation from these overlapped signals demands the application of appropriate signal analysis techniques, which may lead to good reconstruction quality.

1.2 LITERATURE SURVEY

In recent years, many mathematical tools have been developed for the analysis of data in Non-destructive evaluation. Wavelet analysis is one such important technique. Roy et al

[1] have studied the continuous wavelet transform (CWT) applications for signal analysis wherein a disturbing echo of high amplitude is extracted from an experimental ultrasonic signal, which is resulting from a clad state of surface or a side-drilled hole of steel block. Agostino et al [2] utilized wavelet transform for noise suppression to improve ultrasonic flaw detection. The improvement in detection was experimentally verified using steel samples with simulated flaws. Guang-Ming et al [3] performed computer simulation to verify the signal detection improvements for an ultrasonic wave embodied in white noise using cast steel samples with artificial flaws. Later a theoretical model to estimate the optimal frequency–to-bandwidth of the Gaussian wavelet for denoising in ultrasonic NDE is presented [4] with experimental verification.

Castagnede et al [5] analyzed the optimum possibilities offered by correlation method for time of flight measurement when mixing of different modes is present. A criterion for the separation of the different modes, the systematical error associated with their overlapping and an algorithm for unraveling them are also described. Drai et al [6] have developed some signal processing algorithms to facilitate real time processing of ultrasonic NDT data. These algorithms include applications of cross correlation function for planar and volumetric defect discrimination.

Mueller et al [7] discussed several methods of ultrasonic tomography with diffraction effects. Kak [8] reviewed the major developments in imaging with computed tomography (CT) using X-ray emission and ultrasound sources. Errors in reconstruction are used to compare different algorithms, are used by Subbarao et al [9], and it is also found that noise level in the projection data increases the error and slows down the convergence rate in the reconstructed field. The maximum error and RMS error have been found highest in ART and lowest in the MART for given projection data.

1.3 PRESENT WORK

In the present work, the experimental data obtained from an ultrasonic automated scanning setup has been used for tomographic reconstruction of defects of different shapes in various samples. One dimensional discrete wavelet transform was applied for noise suppression from the acquired waveforms. The waveforms received through

inhomogeneity contain two overlapped modes. For separation of these overlapped modes, least-squares method and cross correlation method are presented. A measure of energy-based criterion is suggested to identify the desired mode from the separated modes, whose TOF value is to be considered. This processed time of flight (TOF) is used to reconstruction of the image using computed tomographic (CT) algorithms.

In chapter 2, the details of the experimental setup and data acquisition procedure are discussed.

Chapter 3 presents the wavelet analysis and signal analysis techniques. In this Chapter wavelet application for noise suppression is also given.

Chapter 4 deals with mode separation of multi-path signal using least-squares method and cross correlation method. Time of flight estimation with various criteria is also given in this chapter.

Chapter 5 presents theories of various algebraic reconstruction techniques of computer tomography. Reconstruction of the various domains of the tested samples is also discussed with their images in terms of slowness.

Chapter 6 gives the conclusions of the present work and suggestions for the future work.

Chapter 2

EXPERIMENTAL SET-UP AND PROCEDURE

This Chapter briefly describes the details of the experimental set-up and the aspects of data collection.

2.1 EXPERIMENTAL SETUP

The schematic diagram of ultrasonic automated scanning setup is shown Fig.2.1, to perform A-scan. The present ultrasonic experimental setup, developed in-house (Mahajan [26], Venkatesh [27]), consists of scanning tank, a high resolution type Ultrasonic Flaw Detector (UFD), a high speed data acquisition and other accessories for precision movements of the transducers, data collection and storage. A brief description about the setup is given in the following paragraphs.

2.1.1 SCANNING TANK

The purpose of the scanning tank is to house the stepper motors, the probes and specimen to be tested. As is common practice, the probes and specimens are immersed in water, which acts as a coupling medium. The tank is made up of Perspex plate. Two lead screws, each having pitch of 4 mm, have been fixed in mutually perpendicular directions on a frame located at the top of the tank. The probes mounted on the lead screw could be moved in x-y plane with a step of 1 mm in either direction.

2.1.2 ULTRASONIC FLAW DETECTOR

The Ultrasonic Flaw Detector (UFD) (Krautkrammer-Branson make, USIP12) is used for generating and collecting the ultrasonic signal with the help of probes. The UFD can be used with a single probe in pulse-echo transmission method or with two probes in through-transmission method. The received signal can be obtained from UFD in rectified or radio frequency (RF) mode. There are four controls (for Gain adjustment) by means of which the gain of the received signal can be adjusted to the desired level to reduce noise and avoid any saturation. Various controls are provided for fine adjustments of frequency range, echo shape, pulse repetition frequency, Distance Amplitude Correction (DAC), Monitor adjustment, back wall echo.

2.1.3 COMPUTER

A microcomputer (PC-AT 386SX) is used to control the stepper motors, UFD, A/D converter for data collection and storage.

2.1.4 STEPPER MOTOR AND CONTROLLER

The stepper motor (STM 601 with 12v input) of torque capacity 2kg-cm with maximum step rate of 1023 steps/sec were used. The motor can be moved either clock-wise or anti-clock wise direction through stepper motor control card PCL-211 (manufactured by Dynalog Microsystems). In present setup motors are moved with 50 clock pulses at a time, which corresponds to 1 mm linear movement of the probe.

2.1.5 ANALOG TO DIGITAL CONVERTER

SONTEK STR* 8100 A/D board is used to digitize RF signal from UFD with a maximum data acquisition flexibility through a 64k on-board high-speed memory buffer. The various board functions, under software control, are input channel selection AC/DC coupling, input voltage range, RF/Video made, sampling rates, trigger selection, clock control, threshold phase and level, board selection and interrupt enabling. The board's high-speed data acquisition memory is mapped directly into PC memory space. Once the waveform has been captured, the PC can transfer data off the board at 1.5 MHz rate (8 bit) or 3 MHz rate (16 bit) using simple memory block instructions. This board provides freedom from the static architecture of a stand alone instrument and the computer. The D100A Digital Oscilloscope is used to examine the waveform for selecting the appropriate scan parameters such as delay, gate start, gate length etc. In the present setup the A/D board is installed outside the PC using the PCX-795 PC XT/AT bus expansion system. This board has on-board 1,2,4,8,16 and 32 wait state generation, switch setting for memory bank selection, switch setting for I/O selection and switch setting for DMA channel selection.

2.1.6 TRANSDUCERS

The transducers (probes) used in the present investigation are Immersion Straight Beam probes Z10M, which generate broadband longitudinal waves. They are

connected to the UFD by waterproof connectors. The fixtures were fabricated to hold the transducers in vertical position.

Immersion probes are mainly applied for mechanized or automatic ultrasonic test. In principle they work same as contact probes. A major part of the tests is made in immersion tests tanks filled with water. The diameter of the transducer element is 5 mm (element size). The size of the element strongly affects the shape of the transmitted sound field. The probe has nominal frequency of 10MHz. The frequency has a great influence on the evaluation of reflectors with increasing frequency, the echo height from non-vertically positioned reflectors to the sound beam decreases.

2.2 EXPERIMENTAL PROCEDURE

In the present work, the various specimens tested are given in the following Table. 2.1.

Table 2.1

S. No.	Material		Longitudinal wave Velocity (m/s)		Fig. No.
	Body	Insert	Body	Insert	
1	Perspex	Epoxy*	2730	2650	2.2(a)
2	Nylon	Epoxy	2300	2650	2.2(b)
3	Perspex	Epoxy	2730	2650	2.2(c)
4	Nylon	Epoxy	2300	2650	2.2(d)
5	Perspex	Aluminium	2730	6320	2.2(e)
6	Nylon	Epoxy	2300	2650	2.2(f)
7	Perspex	Epoxy	2730	2650	2.2(g)

* Epoxy resin is LY556 epoxy cured with 10% by weight of hardener HY951, supplied by Ciba-Geigy of India ltd.

The specimen to be investigated is cleaned and area under investigation is marked. Then, the specimen is positioned between the Transmitter and Receiver as shown in fig.2.3. Probes are brought to start position by moving the motor. The gap between the specimen plate surface and the probe surface are adjusted, so as to distinctly observe the initial burst on the UFD oscilloscope screen. The gain adjustment controls are so adjusted that the peak of the signal does not exceed 80% of the maximum screen height of the UFD to avoid saturation. The RF signals from UFD

can be also viewed on the digital oscilloscope provided by the software of the A/D board. The gate parameters on the signal to be digitized are made in data file. In these experiments, the data collection is in one dimension only.

A master control code (in C-language) has been developed for the present investigation controls precise movements of stepper motors and controls the A/D card to collect received waveform in the digitized form. The code is also capable to extract different time and frequency domain features of the waveform during scanning. The initial settings, such as channels, AC/DC coupling, clock source (Intern/Extern), sampling rate (100/200/300/400), trigger type (off/on), post trigger delay, buffer start, buffer length, horizontal delay, gate start, gate length, xfer type (8/16) are set in a data file prior to the execution of the code.

2.2 CLOSURE

In this Chapter the details of experimental setup and procedure were presented. Different components like scanning tank, ultrasonic flaw detector, computer, stepper motor, stepper motor controller, analog to digital converter and transducer were explained. Experimental procedure for data acquisition was also explained.

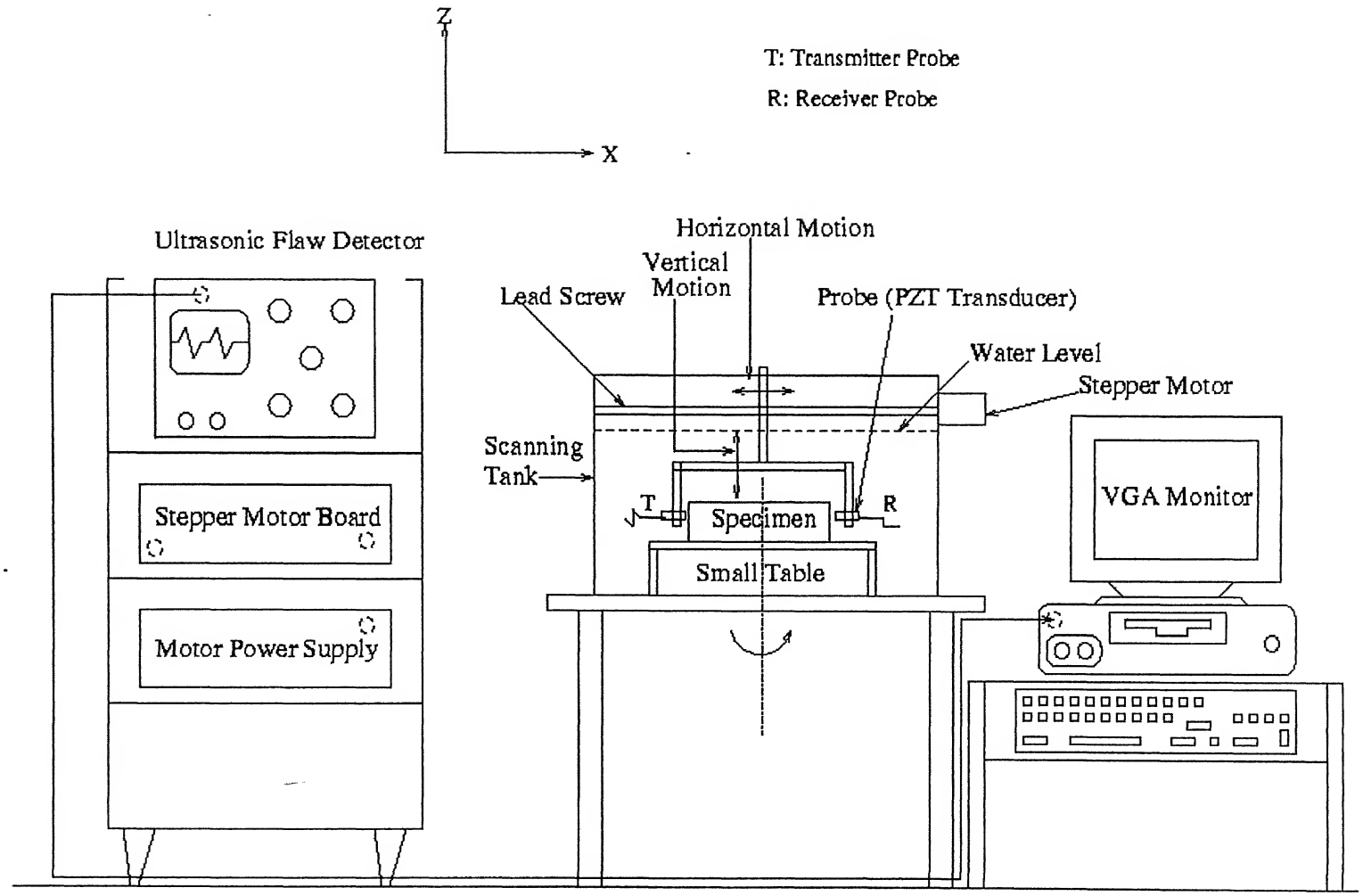

Fig. 2.1. Schematic Diagram of Ultrasonic Automated Scanning Set-up

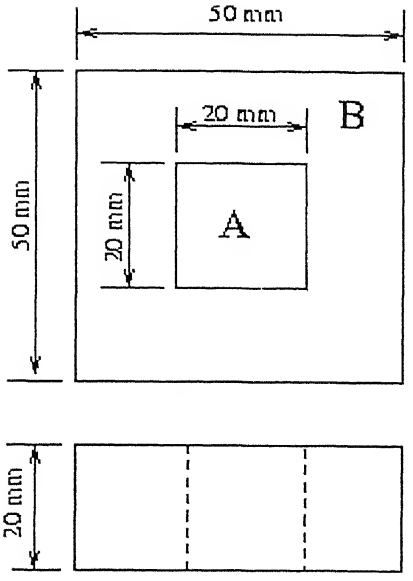

(a) SAMPLE 1
A– Epoxy Resin, B– Perspex

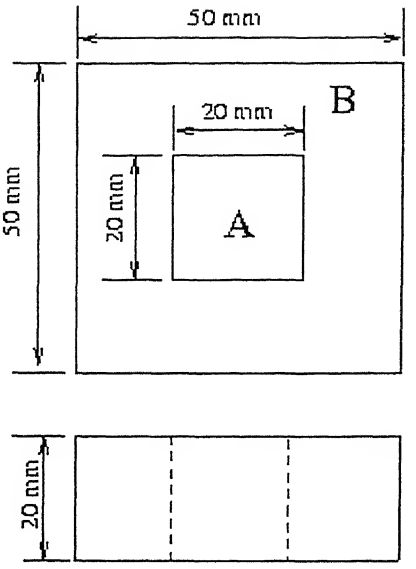

(b) SAMPLE 2
A– Epoxy Resin, B–Nylon

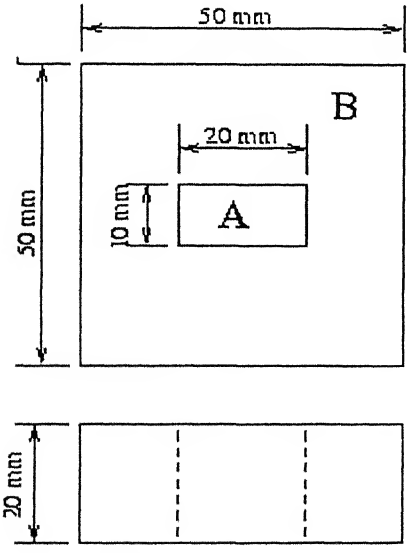

(c) SAMPLE 3
A–Epoxy Resin, B– Perspex

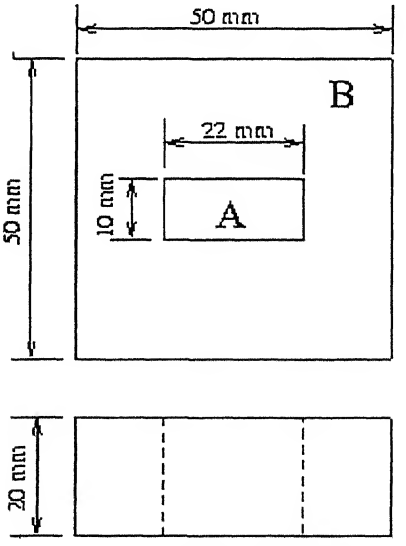

(d) SAMPLE 4
A– Epoxy Resin, B– Nylon

Figs. 2.2(a-d). Different Type of Samples used for the Present work

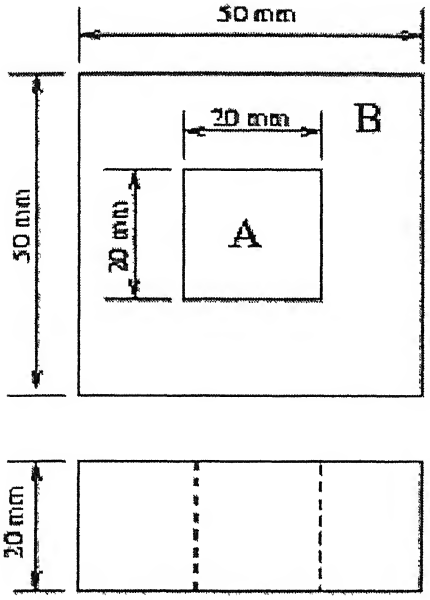

(e) SAMPLE 5
A– Aluminium, B– Perspex

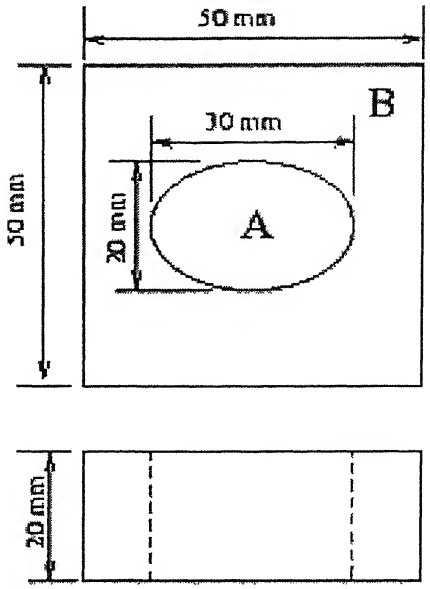

(f) SAMPLE 6
A– Epoxy Resin, B–Nylon

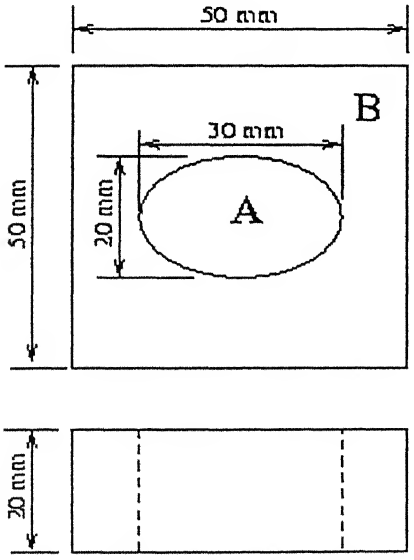

(g) SAMPLE 7
A– Epoxy Resin, B–Perspex

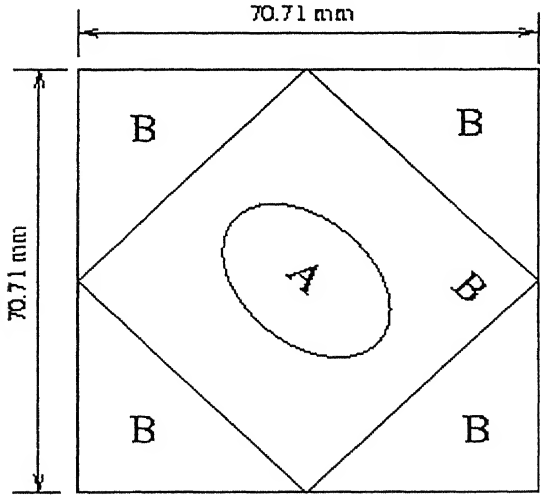

(h) Setup for collecting DATA at 45 and 135 degrees for SAMPLE 7
A– Epoxy Resin, B–Perspex

Figs. 2.2(e-h). Different Type of Samples used for the Present work

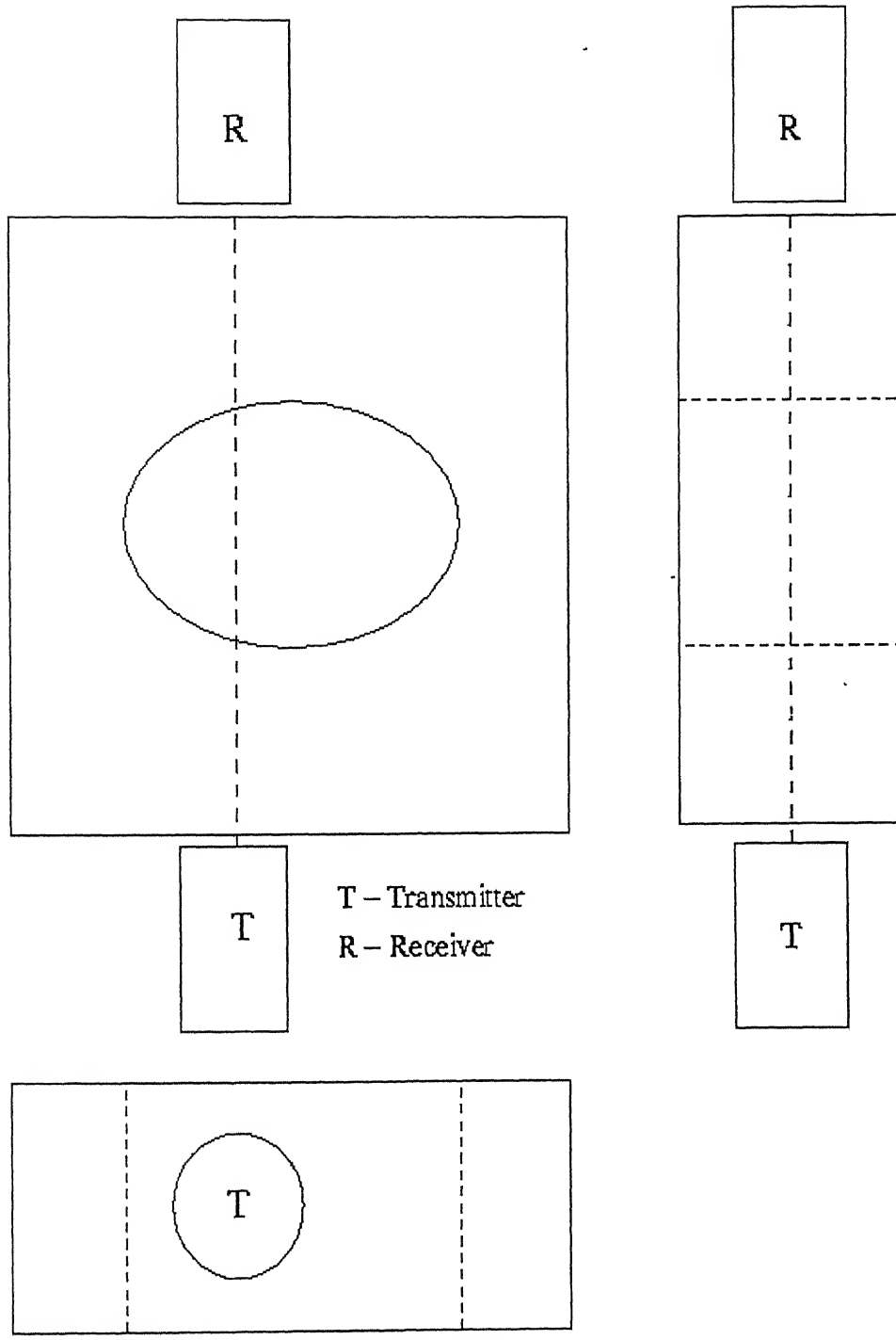

Fig. 2.3. Positions of Transmitter and Receiver for data acquisition

Chapter 3

NOISE SUPPRESSION USING WAVELET TRANSFORM: A SIGNAL PROCESSOR

3.1 INTRODUCTION

Signal processing has become an essential part of contemporary scientific and technological investigation. Signal processing is used in telecommunications, in the transmission and analysis of satellite images, and in medical imaging (echo graph, topography and magnetic resonance), all of which involve the analysis and interpretation of complex time series. In the recent times, this technique is also being applied in Non-destructive Evaluation (NDE) of materials.

The specific goals of signal processing in NDE are.

- To improve inspection reliability,
- To improve defect detection,
- To improve defect characterization, and
- To generate information about the material properties to asses residual life of a structure.

The *Wavelet Transform* (WT) is a recent mathematical technique for processing signals with time-varying spectra, has excellent characteristics of time-frequency localization. Wavelet analysis has wide applications in earthquake prediction, signal processing, image compression, turbulence, non-destructive evaluation (NDE) etc.. In the following sections, the basic operations of wavelet transform are presented.

3.2 BASIC SIGNAL ANALYSIS TECHNIQUES

3.2.1 FOURIER ANALYSIS

Fourier analysis is well known technique of signal processing, which breaks down the signal into constituent sinusoids of different frequencies.

The *Fourier Transform* (FT) is a technique to transform time-domain signal f(t) into frequency- domain signal F(ω). Fig.3.1 shows an example of the *Fourier Transform*. Mathematically the *Fourier Transform* is given by

$$F(\omega) = \int_{-\infty}^{\infty} f(t).e^{-i\omega t}.dt \tag{3.1}$$

and its inverse,

$$f(t) = \int_{-\infty}^{\infty} F(\omega).e^{i\omega t}.d\omega \tag{3.2}$$

where, ω is the frequency.

In *Fourier Transform,* the main drawback is that the time information is hidden. When looking at a FT of a signal, it cannot be seen when the particular spectral components appear exactly in the signal.

3.2.2 SHORT TIME FOURIER ANALYSIS (STFA)

Short-Time Fourier Transform (STFT) is a modification of the Fourier transform. STFT has adapted by *Dennis Gabor* (1946), to analyze a small section of the signal at a time, a technique is called *widowing* a signal. Fig. 3.2(a) shows transformation of a signal into two-dimensional function of time and frequency. Mathematically the STFT, with window function $w(t-\tau)$ is expressed as

$$STFT(\omega) = \int_{-\infty}^{\infty} f(t).w(t-\tau).e^{i\omega t}.dt \tag{3.3}$$

where, $w(t-\tau)$ is the analysis filter or analysis window.

The STFT represents a compromise between the time-domain and frequency-domain views of a signal. It provides information about frequency content in the window of the signal at the given time. However, this information is obtained with limited precision, and that precision is determined by the size of the window. The drawback is that once a particular size is chosen for the time window, that window is the same for all frequencies. Many signals require a more flexible approach, where the window size can vary to determine more accurately in either time-domain or frequency-domain.

3.2.3 WAVELET ANALYSIS (WA)

Wavelet Analysis is the next logical step in which the windowing technique with variable sized regions is used. Wavelet analysis allows both low frequency information with long time intervals and high frequency information with shorter regions. Fig. 3.2(b) shows that wavelet analysis does not use a time-frequency region, but rather a time-scale region. Mathematically, the *Wavelet Transform* (WT) of a signal is defined as follows:

$$W_f(a,b) = \int_{-\infty}^{\infty} f(t).\frac{1}{\sqrt{a}}\psi\left(\frac{t-b}{a}\right).dt \qquad (3.4)$$

where, $\psi(t)$ is a mother wavelet, b is a time shift parameter and a is a scaling parameter. By definition, the WT is the correlation between the signal and set of basic *Wavelets*.

Wavelet analysis produces a time-scale view of a signal, with scaling and shifting. *Scaling* a *Wavelet* means stretching (or compressing) it. Fig. 3.3 shows wavelets with different scaling parameters. Shifting a Wavelet simply means delaying (or hastening) its onset. Mathematically, delaying a function $f(t)$ by τ is represented by $f(t-\tau)$. Fig. 3.4 shows wavelets with different shift factors.

Wavelet analysis is capable of revealing aspects of data that other signal analysis techniques miss such as trends, break down points, discontinuities in the higher derivatives and self-similarity. Wavelet analysis can *compress or de-noise* a signal without appreciable degradation.

Wavelet analysis can be performed in two ways

1. Using continuously translated and dilated versions of mother wavelet (CWT), or
2. Using discretely translated and dilated versions of mother wavelet (DWT).

3.2.3.1 Continuous Wavelet Transform (CWT)

The continuous wavelet transform (CWT) is defined as the sum over all time of the signal multiplied by scaled and shifted versions of the wavelet function ψ, which can be represented as

$$C(a,b) = \int_{-\infty}^{\infty} f(t)\psi^{*}_{a,b}(t)\ dt \tag{3.5}$$

where, C (a, b) are the coefficients of the wavelet transform, f*(t)* is the signal being analyzed and * denotes the complex conjugate of $\psi_{a,b}$. Here, $\psi_{a,b}$ is the shifted and scaled version of the mother wavelet $\psi(t)$ as given by,

$$\psi_{a,b} = a^{-1/2}\psi\left(\frac{t-a}{b}\right), \quad (a,b) \in R^2, \quad a > 0 \tag{3.5a}$$

The word continuous in CWT means, that the transform operates the wavelets on the signal with continuous in scaling and shifting. During the computation, the analyzing wavelet is shifted smoothly over the full domain of the analyzed signal/function.

3.2.3.2 Discrete Wavelet Transform (DWT)

Calculating Wavelet coefficients in CWT at every possible scale generates a very large amount of data. This disadvantage of CWT is overcome by choosing scales and positions based on powers of two, so called dyadic scales and position, which is more efficient and just as accurate. Such an analysis is called Discrete Wavelet Transform (DWT). The generation of the wavelets and calculation of the DWT are well matched to digital computer.

The wavelet transform can also be expressed in discrete form

$$f(t) = A\sum_{m}\sum_{n} C_{m,n}\psi\left(\frac{t - na_0^m T}{a_0^m}\right) \tag{3.6}$$

where,

$$C_{m,n} = a_0^{-m/2}\int f(t).\psi\left(\frac{t - na_0^m T}{a_0^m}\right).dt \tag{3.7}$$

$$a = a_0^m \tag{3.8}$$

$$b = na_0^m T \tag{3.9}$$

where, T is the sampling period, A and a_0 are constants, where a_0=2 for the dyadic wavelet transform, m is depend upon the number of decomposition levels and n is depend upon the length of the signal to be decomposed.

Multi Resolution Analysis (MRA)

Multi resolution wavelet analysis allows the decomposition of a function/signal in progression of successive *approximation* and *details*, corresponding to different scales. The *approximations* are high-scale, low frequency components and the *details* are the low-scale, high frequency components of the signal. The difference between the actual signal and its approximation of order n is called its *residual.* Intuitively, the *approximation* is relatively smooth, and *detail* being composed of high frequency components. The *detail* corresponds to the difference between two successive levels of approximation.

Multiple-Level Decomposition

In DWT, the decomposition process can be iterated, with successive approximations being decomposed in turn, so that one signal can be broken into many lower-resolution components. This is called the *Wavelet decomposition tree*. Fig. 3.5 shows the Multi-level (three level) wavelet decomposition tree.

Wavelet Reconstruction

Wavelet reconstruction, or *synthesis* is the process of reconstructing the decomposed signal using a set of decomposed coefficients. The mathematical manipulation that effects synthesis is called the *inverse discrete wavelet transform* (IDWT).

3.2.3.3 Properties of Wavelets

The best-performing *mother wavelet* should have the following three properties.

1. The admissible condition is given by

$$\int_{-\infty}^{\infty} \psi(t)\, dt = 0 \tag{3.10}$$

2. The wavelet has the characteristic of good time-frequency localization. This property makes the wavelet transform is powerful tool for analysis of non-stationary signals such as sound, seismic, electromagnetic signals etc.

3. The power spectrum of the wavelet is well matched with that of the signal to be analyzed.

3.2.3.4 Different types of Wavelets

A wavelet is a waveform of limited duration, which has the above properties. Different types of mother wavelets are discussed in the following paragraphs.

The simplest wavelet is *Haar* wavelet, which is a step function (Figs. 3.6(a) and 3.6(b)).

Ingrid *Daubechies*, one of the brightest stars in the world of wavelet research, invented what are called compactly supported orthonormal wavelets. The names of the *Daubechies* family wavelets are written as *dbN*, where N is the order, and *db* is the "surname" of the wavelet. The *db1* wavelet is same as *Haar*. Figs. 3.6(c) through 3.6(p) shows the scaling and wavelet functions of the various Daubechies wavelets.

In *Biorthogonal* wavelets two types of wavelet functions are used: one for decomposition and other for reconstruction instead of the same one. *Coiflets, Symlets, Morlet, Mexican Hat, Mayer* etc. are other different type of wavelets suitable for various purposes.

There are different wavelets that can be used to decompose the signal and extract feature vector. These wavelets include Daubechies (db1-db10), Biorthogonal (bior1.3-bior6.8), symlets (sym2-sym8), coiflets (coif1-coif5), Morlet, Mexican hat and Meyer. The criterion for selection of the proper mother wavelet is based on the shape of the wavelet function, which could match well with the shape of the signal mode to be analyzed. In the present work, Daubechies, order 5 ('db5') has been chosen, because it seems to match with the signal mode to be analyzed and also it posses a good time-frequency localization. Figs. 3.6(a) to 3.6(p) shows different type of wavelet and scaling functions. Fig. 3.6(j) shows the Daubechies-5 ('db5') that has been used in the present work.

3.3 NOISE SUPPRESSION

In Ultrasonic Nondestructive Evaluation (NDE), the observed ultrasonic signal *S(t)* can be expressed as the sum of the two components.

$$s(t) = y(t) + n(t) \tag{3.11}$$

where, *y(t)* is the reflected signal of the defect and *n(t)* is the noise. Removal noise is extremely important in the ultrasonic defect detection to identify the defects correctly.

The main steps of the signal noise removal are.

1. Decomposition of the signal into coefficients,
2. Separation of the *approximation* and *detail* coefficients from the coefficients, and
3. Reconstruction of the de-noised signal from the *approximation* coefficients and their different levels of the noises from the *detail* coefficients.

A code is developed for the noise suppression from the signal is given in the *appendix A*. In this, the analysis is limited to 3-level decomposition of the signal. In 3-level decomposition, the function *wavedec* (in the MATLAB toolbox) returns the coefficients of all the components (i.e. third-level approximation and first three levels of details) and concatenated into one vector, C. Vector L gives the lengths of each component. In the second step, the coefficients of approximation and details have been extracted from decomposed vector, C. In the third step, the de-noised signal (approximation) and the three levels of noises (details) have been reconstructed from their corresponding coefficients. Fig. 3.7 shows various levels of suppressed noises (details) and de-noised signal (approximation) of a non-overlapped signal, which is received through an Epoxy inserted Perspex sample with 3-level decomposition. As the level of decomposition increases, the frequency of the detail (noise) decreases. Figs. 3.8 and 3.9 show the noise suppression of the overlapped signals, which are received through region of in-homogeneity of samples Epoxy inserted Nylon sample and Epoxy inserted Perspex sample respectively. In fig. 3.10, the original signal is an overlap of two modes with very small time shift, which is received through a region of in-homogeneity of Perspex sample with Epoxy resin rectangular insertion of 20mm×10mm. In this figure the de-noised signal (approximation) looks like a single mode signal, just after 1-level decomposition. The signal has lost some important information (i.e. two peaks of two different modes). This is the limitation for the noise suppression. So, the de-noising characteristics depend on the level of decomposition and signal to be analyzed. Therefore, in the present work, different levels have been chosen for different signals according to their shapes.

3.4 CLOSURE

In this Chapter, the basis of FT, STFT and Wavelet Transform (WT) have been presented. Some of the important mother wavelets and their properties have been discussed. Noise removal using multi-level DWT, which has been used in the present work, has also been explained.

Fig. 3.1 Fourier Transform for transforming a time-domain signal to frequency-domain

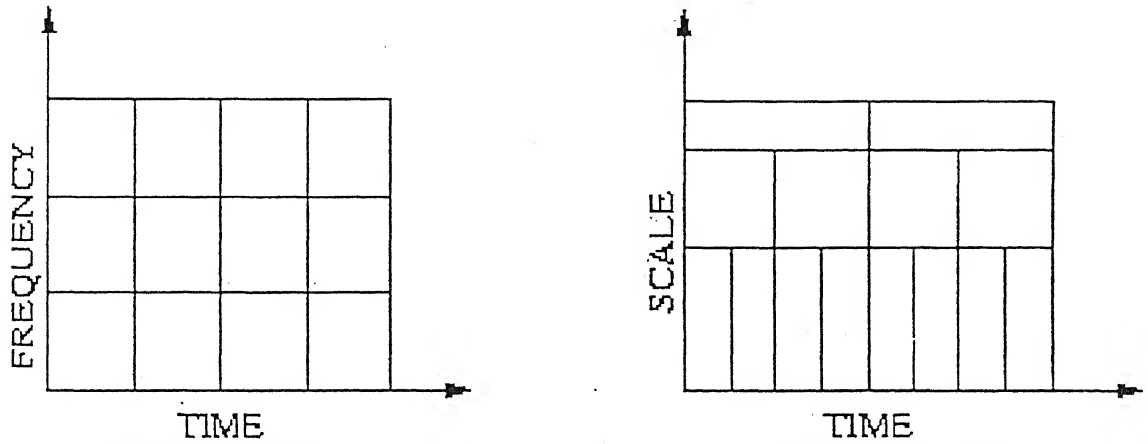

(a) STFT (Gabor) (b) Wavelet Analysis

Figs. 3.2(a-b) Short-Time Transform (Time-frequency domain) and Wavelet Transform (Time-scale domain)

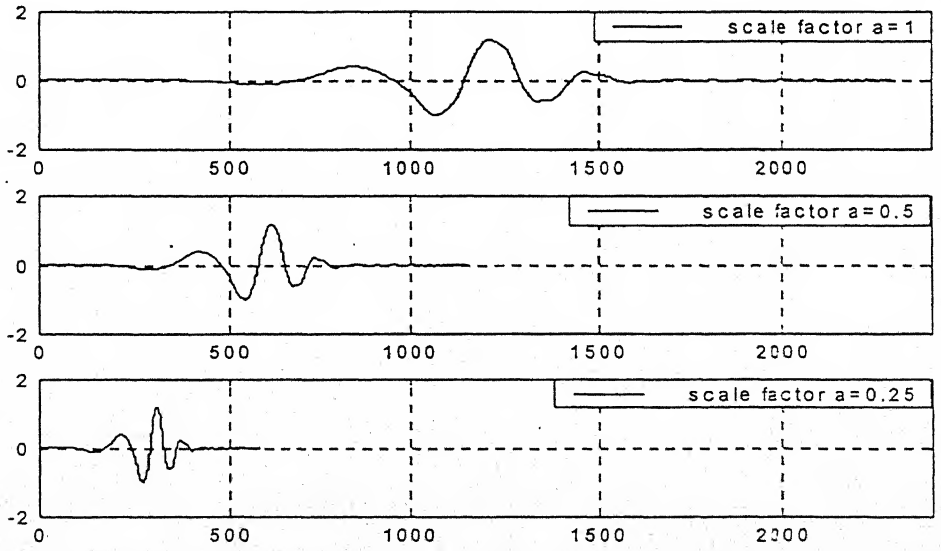

Fig. 3.3 Scaling (stretching or compression) of the wavelets with different scale factors

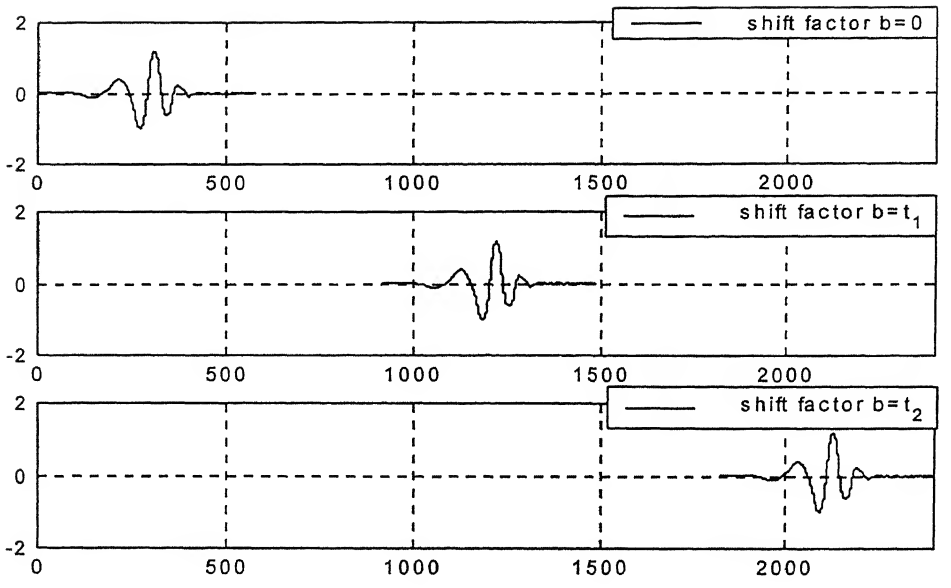

Fig. 3.4 Shifting (delaying or hastening) of the wavelets with different shift parameters

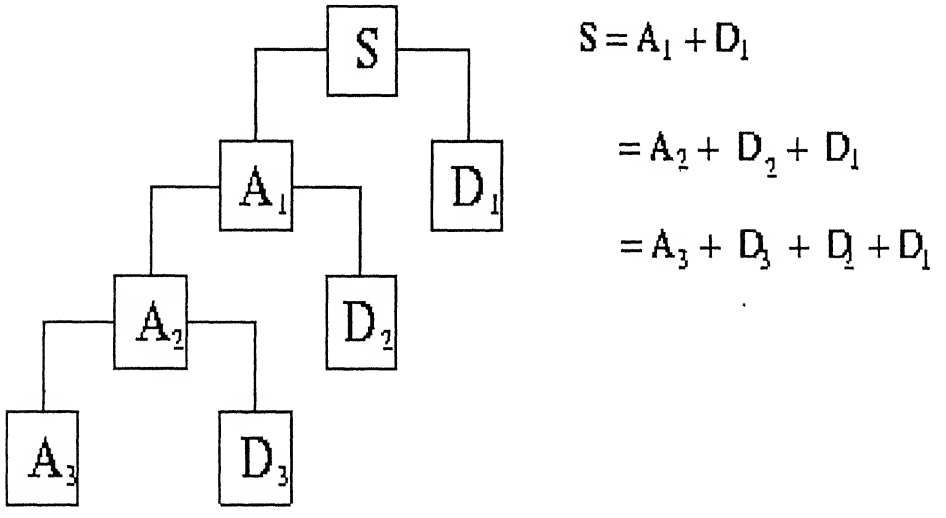

Fig 3.5 Multiple-Level Wavelet decomposition tree with three-level decomposition

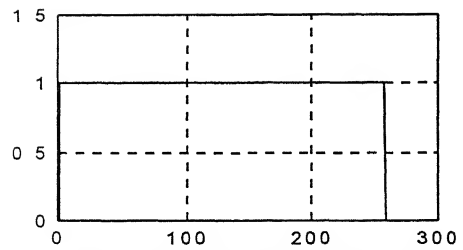

(a) db1/Haar Scaling function

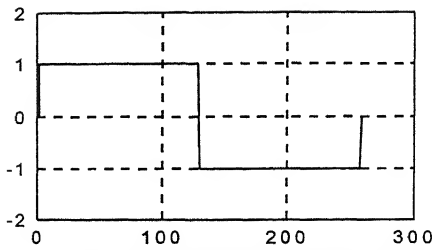

(b) db1/Haar Wavelet function

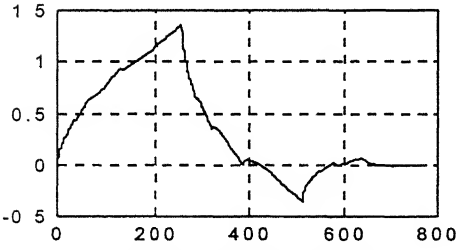

(c) db2 Scaling function

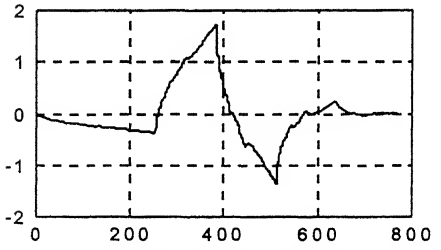

(d) db2 Wavelet function

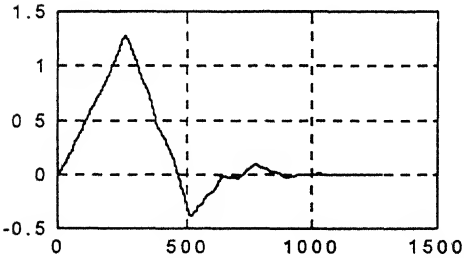

(e) db3 Scaling function

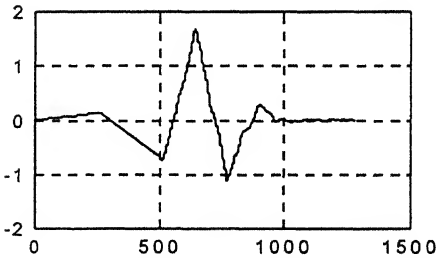

(f) db3 Wavelet function

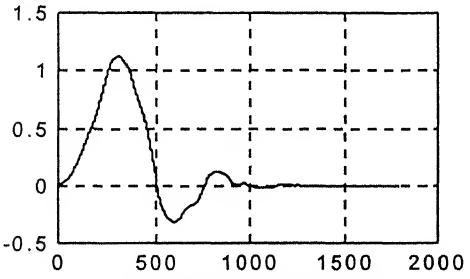

(g) db4 Scaling function

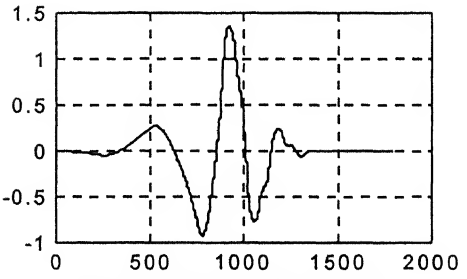

(h) db4 Wavelet function

Figs. 3.6(a-h) Different wavelets (Daubechies) scaling and wavelet functions

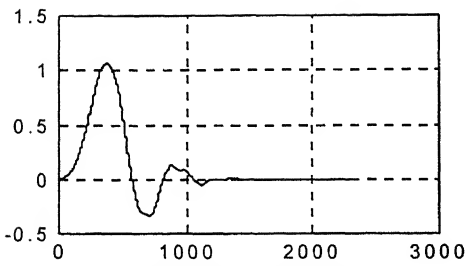

(i) db5 Scaling function

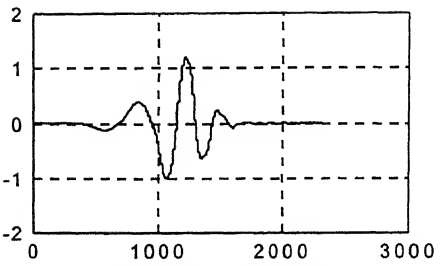

(j) db5 Wavelet function

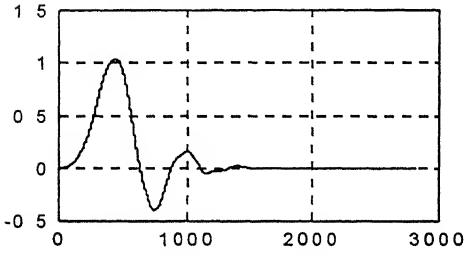

(k) db6 Scaling function

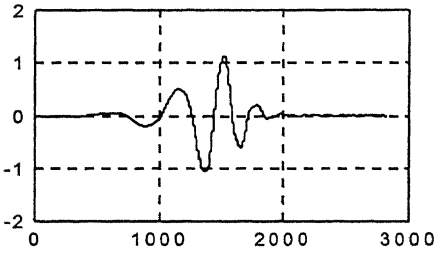

(l) db6 Wavelet function

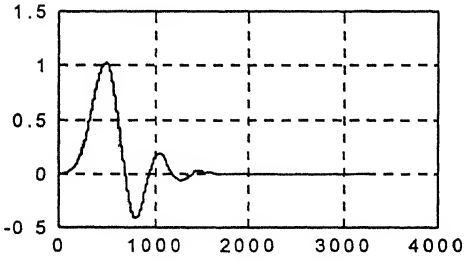

(m) db7 Scaling function

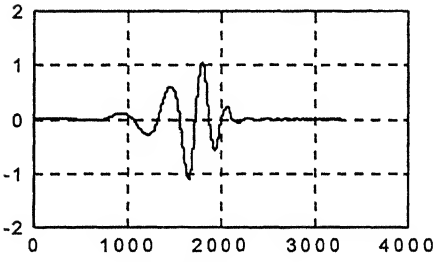

(n) db7 Wavelet function

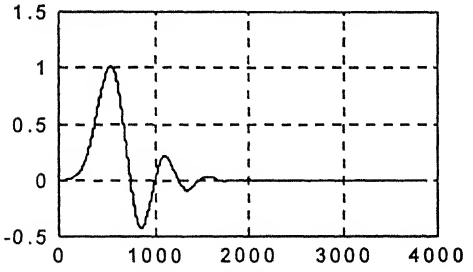

(o) db8 Scaling function

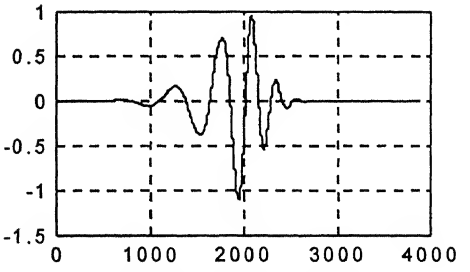

(p) db8 Wavelet function

Figs. 3.6(i-p) Different wavelets (Daubechies) scaling and wavelet functions

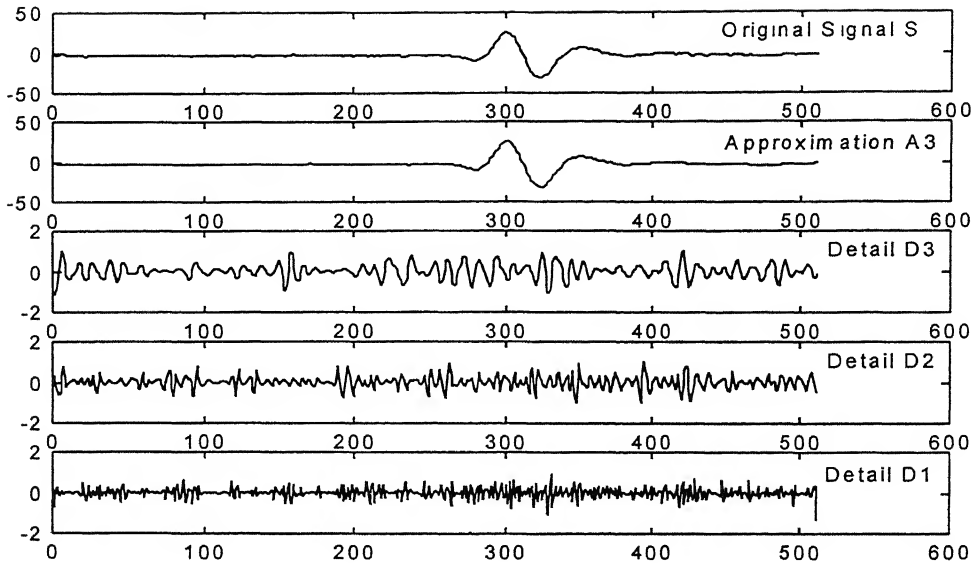

Fig. 3.7 Wavelet 3-level decomposition of a signal through rectangular insertion of 20mm×20mm (Epoxy resin) in Nylon sample with 'db5' wavelet

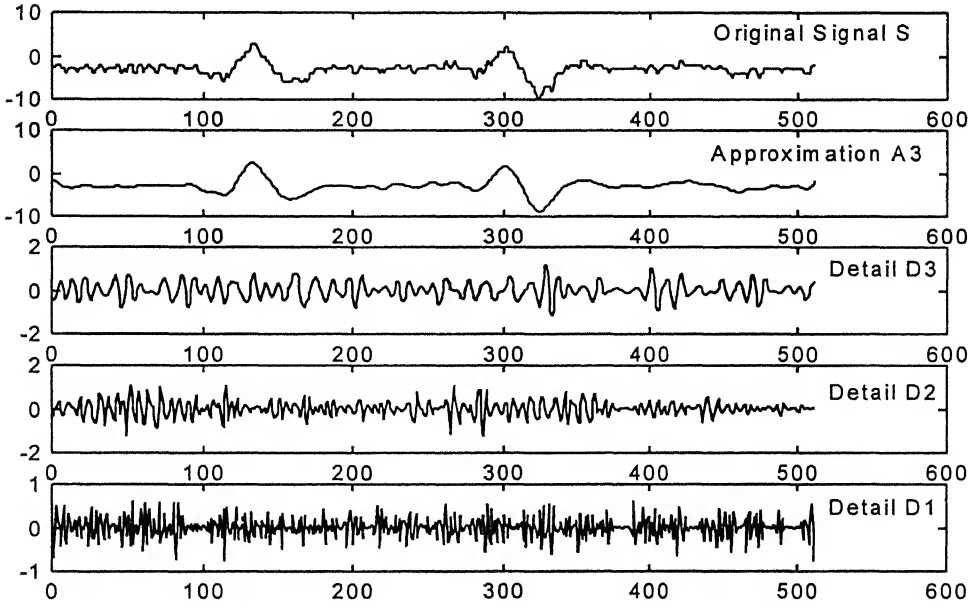

Fig. 3.8 Wavelet 3-level decomposition of overlapped signal at border of rectangular insertion of 20mm×20mm (Epoxy resin) in Nylon sample with 'db5' wavelet

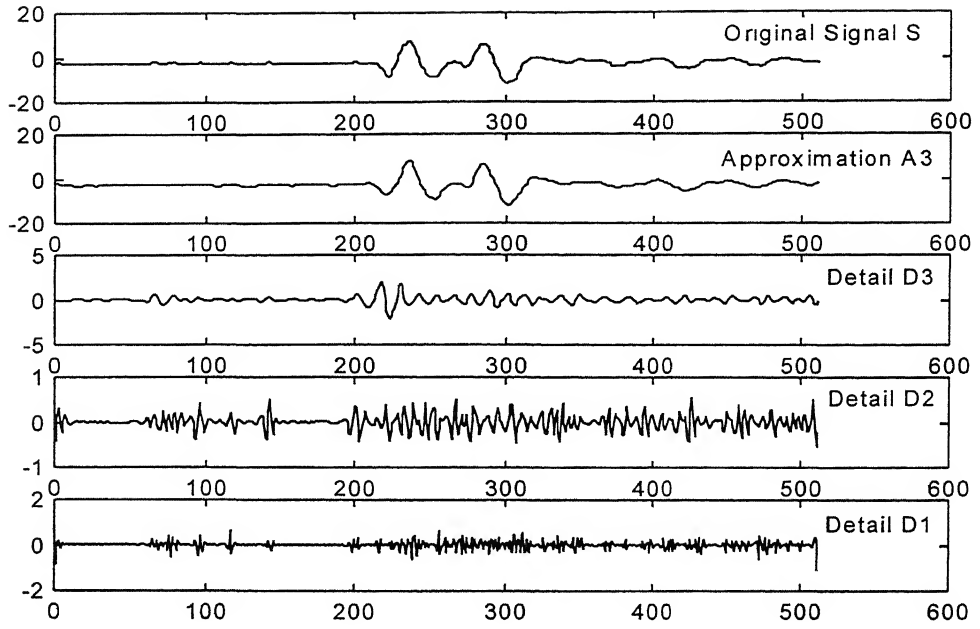

Fig. 3.9 Wavelet 3-level decomposition of overlapped signal at border of rectangular insertion of 20mm×20mm (Epoxy resin) in Perspex sample with 'db5' wavelet

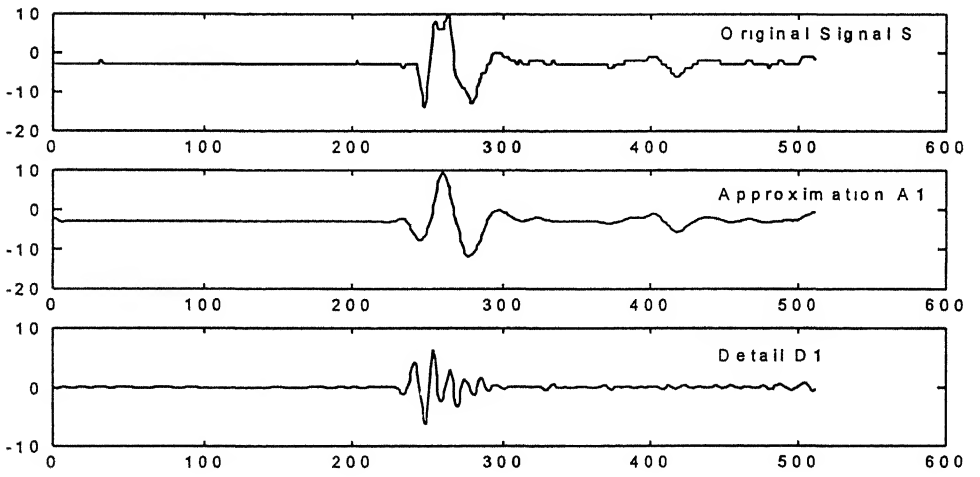

Fig. 3.10 Wavelet 1-level decomposition of overlapped signal at border of rectangular insertion of 20mm×10mm (Epoxy resin) in Perspex sample with 'db5' wavelet

Chapter 4

RESOLUTION OF INDIVIDUAL MODES IN A MULTI-PATH SIGNAL AND TIME OF FLIGHT ESIMATION

4.1 INTRODUCTION

In many applications such as radar and sonar data processing, geological acoustic sounding, ultrasound based non-destructive testing, and medical imaging procedures the determination of certain event times is faced with the problem of resolving unknown number of close spaced, overlapping and noisy echoes of a signal with known shape. When a signal is passing through solid-solid interface, the signal path splits into two or more paths and arrives at the receiver at different times. Thus, the signal is collected at the receiver is superposition of these individual signal modes and is called overlapped or multi-path signal. In figs. 4.1(a), 4.2(a), 4.3(a) and 4.4(a) show the multi-paths of various samples. In all these cases, when the signal is passes through the border of in-homogeneity the signal path splits in to two separate paths and reach the receiver and plot as an overlapped or multi-path signal with some time-shift. These types of multi-path signals have been observed in the present work. Then the received multi-path *S(t)* signal can be described mathematically as

$$S(t) = \sum_{i=1}^{N} A_i R(t - \tau_i) + n(t) \tag{4.1}$$

where, A_i and τ_i are the amplitudes and arrival times respectively, for the *i*th multi-path signal, N is the number of multi-paths, R(t) is representative reference signal from a path and n(t) is the additive noise.

In the previous chapter, about suppression of additive noise has been discussed. After the removal of the noise, the de-noised signal *S(t)* becomes,

$$S(t) = \sum_{i=1}^{N} A_i R(t - \tau_i) \tag{4.2}$$

The experimental de-noised signals at various potions are shown in figs. 4.1 to 4.4. Fig. 4.1(a) shows a Perspex sample of 50mm×50mm size with square insertion

(Epoxy resin) of 20mm×20mm. Fig. 4.1(b) shows received signals at three different positions of location shown in fig. 4.1(a). It can be seen that the signal has only one mode when it passes through the complete homogeneous material. If it passes through the interface region of the in-homogeneity, the signal is a multi-path signal with two signal modes as shown in fig. 4.1(b). If the sound velocity through insert material is faster than the base material, then the signals are as shown in figs. 4.1(c) and 4.1(d). In fig 4.1(d), the two signal modes with more time shift, because the sound velocity difference between the base material (Perspex) and inserted material (Aluminium) is very high. When the insertion thickness is small the multi path signal are overlapped closely as shown fig. 4.2(b) for sample shown in fig. 4.2(a).

In real practice perfect rectangular/square insertions exist rarely. So, the present work focuses on elliptical insertion as shown in fig. 4.3(a). Figs. 4.3(b) and 4.3(c) show signals for various positions of the transmitter for the case of Epoxy resin inserted in Nylon sample and Perspex sample with Epoxy resin insertion.

Time of flight (TOF) is the important parameter in NDT. In the present work, for separating the different modes of the multi-path signal, two different types of algorithms have been used. The methods are

1. A Least-squares method algorithm for resolution of multi path signal, and
2. Cross correlation method using Fast Fourier Transform (FFT) has been used, when only one reference (single path) signal is available.

4.2 LEAST-SQUARES (LS) METHOD

The method of *Least squares* is systematic procedure to fit a unique curve through given data points. In the present work, the multi-path signal (overlap of two modes) is separated with the help of reference (single path) signals.

Let the received signal *S(t)* be assumed to consist of two modes. Then *S(t)* can be represented as,

$$S(t) = A_1 R_1(t) + A_2 R_2(t) + A_3 \tag{4.3}$$

where, $R_1(t)$ and $R_2(t)$ are two reference signals, A_1 and A_2 are amplitudes of the modes, and A_3 is DC-offset of the signal from the time axis. If e_j is the error of approximation at j^{th} point, then

$$e_j = S_j - \left(A_1(R_1)_j + A_2(R_2)_j + A_3\right) \tag{4.4}$$

If the signal is descritized at M points, then total square error equation can be written as,

$$E = \sum_{j=1}^{M}\left[S_j - \left(A_1(R_1(t))_j + A_2(R_2(t))_j + A_3\right)\right]^2$$

$$= \sum_{j=1}^{M} e_j^2 \tag{4.5}$$

Then, the method of least squares consists of determining such that the error E is minimized.

For E to be minimum, the conditions are

$$\frac{\partial E}{\partial A_1} = 0 = \sum_{j=1}^{M} -2(R_1)_j\left[S_j - \left(A_1(R_1)_j + A_2(R_2)_j + A_3\right)\right], \tag{4.6a}$$

$$\frac{\partial E}{\partial A_2} = 0 = \sum_{j=1}^{M} -2(R_2)_j\left[S_j - \left(A_1(R_1)_j + A_2(R_2)_j + A_3\right)\right], \text{ and} \tag{4.6b}$$

$$\frac{\partial E}{\partial A_3} = 0 = \sum -2.\left[S_j - \left(A_1(R_1)_j + A_2(R_2)_j + A_3\right)\right] \tag{4.6c}$$

The above equations in the matrix notation, is given as

$$[F]\{A\} = \{G\} \tag{4.7}$$

where,

$$[F] = \begin{bmatrix} F_{11}F_{12}F_{13} \\ F_{21}F_{22}F_{23} \\ F_{31}F_{32}F_{33} \end{bmatrix}, \quad \{A\} = \begin{Bmatrix} A_1 \\ A_2 \\ A_3 \end{Bmatrix}, \text{ and } \{G\} = \begin{Bmatrix} G_1 \\ G_2 \\ G_3 \end{Bmatrix}$$

where,

$$F_{11} = \sum_{j=1}^{M}(R_1)_j^2, \; F_{22} = \sum_{j=1}^{M}(R_2)_j^2, \; F_{33} = \sum_{j=1}^{M}1 = M,$$

$$F_{12} = F_{21} = \sum_{j=1}^{M}(R_1)_j(R_2)_j, \; F_{13} = F_{31} = \sum_{j=1}^{M}(R_1)_j, \; F_{23} = F_{32} = \sum_{j=1}^{M}(R_2)_j,$$

$$G_1 = \sum_{J=1}^{M} (R_1)_J S_J \text{ , } G_2 = \sum_{J=1}^{M} (R_2)_J S_J \text{ , and } G_3 = \sum_{J=1}^{M} S_J$$

The code developed (in MATLAB) for the present work has been given in *Appendix B*. In this, each signal is a set of 512 data points. At the end A_1R_1 and A_2R_2 give the separated modes of the signal. Figs. 4.5 and 4.6 show the signal modes, which are separated by least-squares method for the overlapped signals of Aluminium inserted Perspex sample and Epoxy resin inserted Perspex sample respectively.

4.3 CROSS CORRELATION METHOD USING FFT

In statistical terms, *correlation* is a measure of the linear relationship between two variables. The correlation between x and y can be written as, Σxy, where x and y are set of independent data points. It is also applicable to deterministic functions such as sinusoids. In the application of the correlation methods to engineering problems, the features generally expressed as waveforms rather than discrete time series. The correlation or covariance is expressed as a function of time delay τ, as

$$C_{xy}(\tau) = \int_{-\infty}^{\infty} x(t)y(t+\tau)dt \tag{4.8}$$

where, τ is the time shift, lag or delay.

If the waveform, x(t) correlate with a time-shift version of itself, is called *Autocorrelation*. Then the equation can be writing as

$$C_x(\tau) = \int_{-\infty}^{\infty} x(t)x(t+\tau)dt \tag{4.9}$$

When a waveform correlate with another waveform, is called *cross correlation*, which describes the dependence between those waveforms. Then, the cross correlation function between waveforms, x(t) and y(t) can be expressed in terms of time shift as given in the equation 4.8.

Correlation using FFT

The correlation between the signals R(t) and S(t) can be written as

$$C_{RS}(\tau) = \int_0^T R(t).S(t+\tau).dt \tag{4.10}$$

where, R(t) is a reference signal, S(t) is the multi path signal and T is the time range. After Fast Fourier Transform (FFT), the equation 4.2 becomes

$$S(\nu) = \sum_{i=1}^{N} A_i.R(\nu).\exp(-2.j.\pi.\tau_i.\nu) \tag{4.11}$$

Then, the equation for p^{th} mode can be written as

$$s_p(\nu) = S(\nu) - \sum_{\substack{i=1 \\ i \neq p}}^{N} A_i.R(\nu).\exp(-2j\pi.\tau_i\nu) \tag{4.12}$$

where, $s_p(\nu)$ is the p^{th} separated mode, $S(\nu)$ and $R(\nu)$ are the FFT of the S(t) and R(t). ν is the frequency array. j indicates complex number. N is the number of modes. The separation of the various modes of the multi path signal has been done as per the flow chart as shown in fig. 4.7. At the end of the each iteration, the values of amplitude and time-shift are updating as per the equations

$$A_p = \sqrt{\frac{\int_{\nu_1}^{\nu_2} |s_p(\nu)|^2 \, d\nu}{\int_{\nu_1}^{\nu_2} |R(\nu)|^2 \, d\nu}} \tag{4.13}$$

and,

$$\tau_p = pos\left[\max\left(F^{-1}\left(s_p(\nu).R(\nu)\right)\right)\right] \tag{4.14}$$

where, F^{-1} indicates Inverse Fast Fourier Transform (IFFT), *max* is for maximum value, *pos* for position for the maximum value index. These values of A_p and τ_p will be using in the next iteration according to the flow chart [5] shown in fig. 4.7 for further updating.

After finding the values of amplitudes and time-shifts for all the modes (N) of the signal, the individual modes can be reconstructed using amplitudes (A_p), time shifts (τ_p) and reference signal (in frequency mode) as per the equation

$$s_i = R(\nu).A_i.\exp(-2j.\pi.\tau_i.\nu), i = 1,2,3,.....N \tag{4.15}$$

where, N is the number of modes in the multi path signal. Appendix C shows the code written in MATLAB language for the present work. Figs 4.8 shows an example of the

reference signals, multi path (signal to be separated) signals, and their separated modes of the signals for sample of Aluminium inserted Perspex sample. In this, the overlapped signal is overlap of two signal modes with large time shift. Fig. 4.9 shows for overlapped signal with overlap of two signal modes with small time shift. Fig. 4.10 shows the separation of overlapped signal with very small time shift when the thick ness of the insertion is reduced. Figs 4.11 and 4.12 show the reference signals, multi path (signal to be separated) signals, and their separated modes of the signals for sample of Perspex with elliptical insertion of Perspex material.

4.4 SELECTION OF DESIRED MODE

After separation of individual modes of a multi-path signal, selection of desired mode from the separated modes of the signal plays major role in the Time of Flight (TOF) measurement. In the present work, a measure of energy criterion has been proposed for this selection. The measure of energy of a signal is defined as the sum of the squares of the signal values. Then the equation of the energy (EN) of the signal (s) having M data points is given as

$$EN = \sum_{i=1}^{M} s_i^2 \tag{4.16}$$

In the present work, the measure of energy of the signals through base material and through insertion are differing a lot. Different attenuation characters of the material and scattering effects at the solid-solid interface may attribute this. So, for selection of desired mode from the separated modes, percentage of energy (normalized energy) of the signals have been taken into consideration rather than energy of the signals. Fig 4.16 and fig 4.17 show the energy of the signal versus probe position and percentage of energy versus probe position respectively. At position 15.5 mm the normalized (or percentage of) energy of the signal mode through insertion is more than the normalized (or percentage of) energy of the signal mode through base material. According to the energy criterion, the signal mode through insertion has been selected as a desired mode for the time of flight data. This energy-based criterion is equally applicable to the situations when the sound velocity in insert material is higher than the base material and vice versa.

4.5 TIME OF FLIGHT ESTIMATION

Time of flight is the important parameter for reconstruction of the ultrasonic image with computer-aided tomography. The equation used for Time of flight data the equation as follows

$$TOF = ptd + t \tag{4.17}$$

where, TOF is the Time of flight in second, ptd is the *post trigger delay* and t is the *time delay* (from an digitized signal). Fig 4.13 shows the post trigger delay and time delay measurements for TOF. In multi path signal, when the normalized energy of the separated signal mode received through insertion is higher than the signal through the base material, then the signal through insertion material has been taken into consideration for Time of flight estimation as shown in figs. 4.14 and 4.15 for the sample, sound velocity of insertion material is lower than base material and for the sample, sound velocity of insertion material is higher than base material respectively.

4.6 CLOSURE

In this Chapter about resolution of multi path signal using least squares method and cross correlation method using FFT are discussed. The energy criterion for selection of desired mode from the separated modes for TOF measurement is also presented.

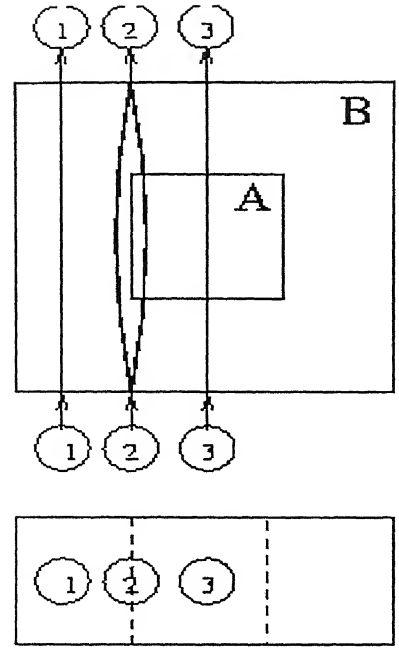

Fig. 4.1(a) Sample-1 of Perspex (B) with 20mm×20mm insertion of Epoxy Resin (A) with three positions of data collection

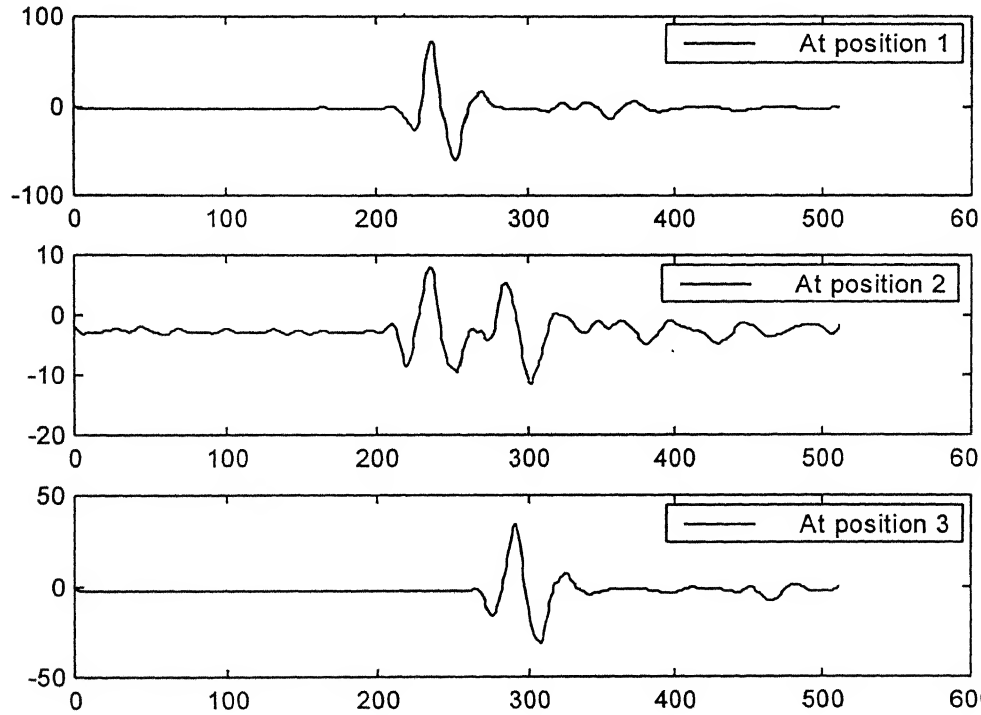

Fig. 4.1(b) Signals at three different positions (i.e. shown in fig. 4.1(a)) for Perspex sample with Epoxy resin insertion of 20mm ×20mm

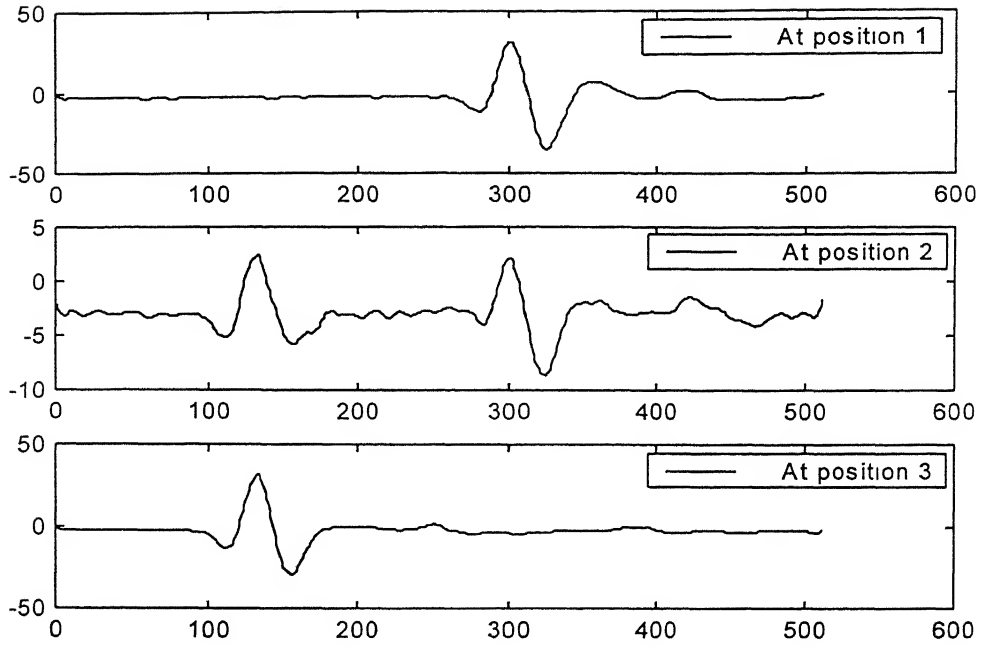

Fig. 4.1(c) Signals at three different positions (i.e. shown in fig. 4.1(a)) for Nylon sample with Epoxy resin insertion of 20mm ×20mm

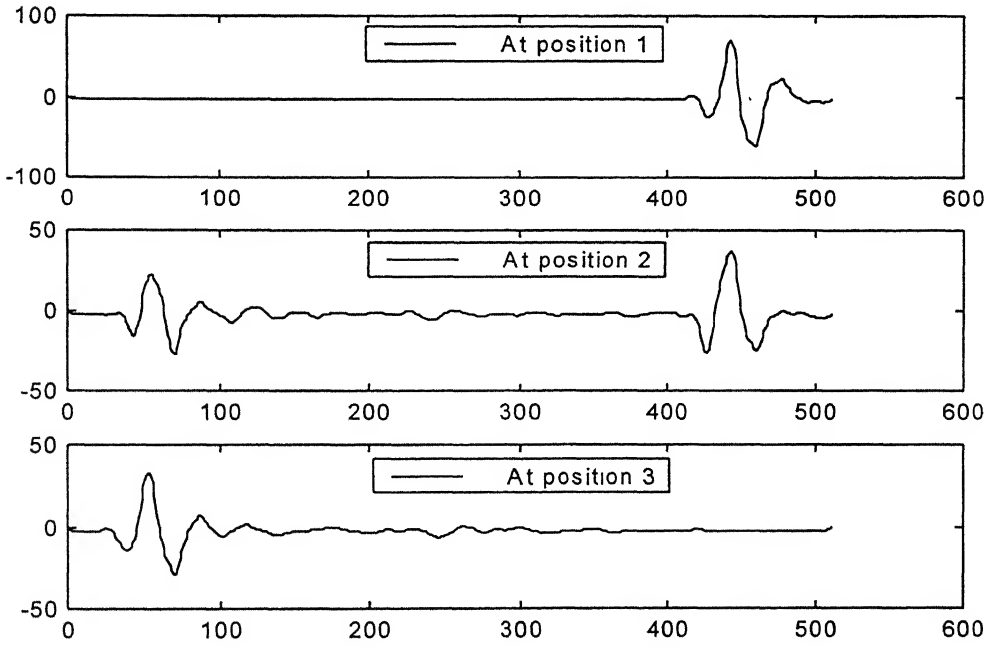

Fig. 4.1(d) Signals at three different positions (i.e. shown in fig. 4.1(a)) for Perspex sample with Aluminium insertion of 20mm ×20mm

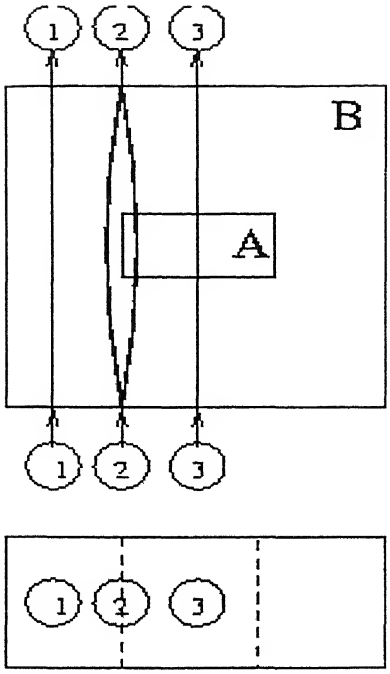

Fig. 4.2 (a) Sample-3 of Perspex (B) with 20mm×10mm insertion of Epoxy Resin (A) with three positions of data collection

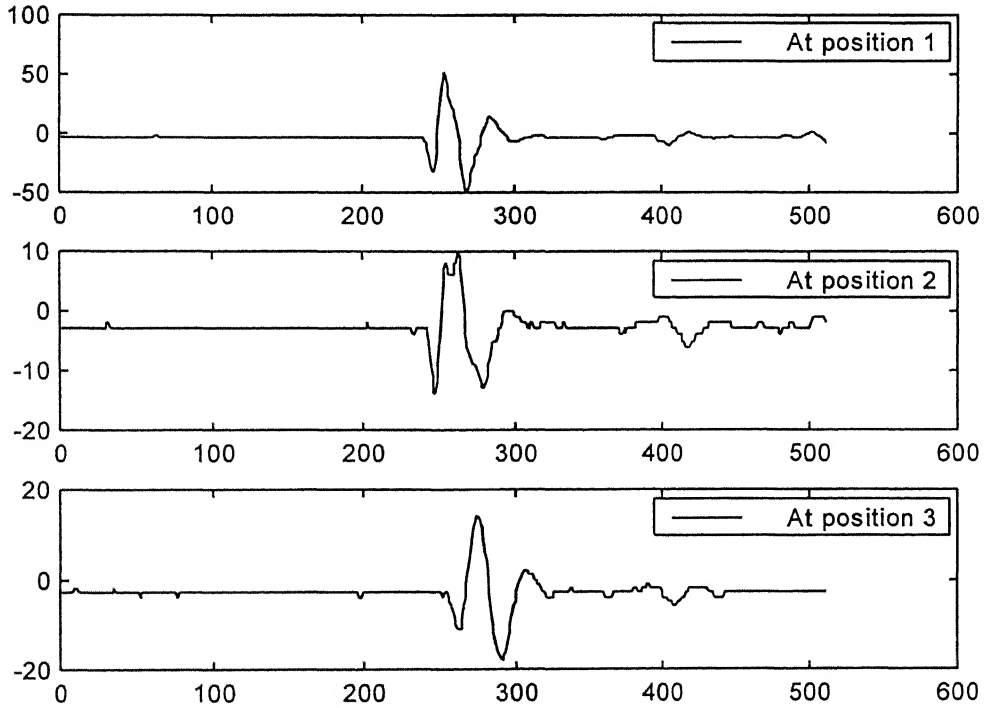

Fig. 4.2(b) Signals at three different positions (i.e. shown in fig. 4.2(a)) for Perspex sample with Epoxy resin insertion of 20mm ×10mm

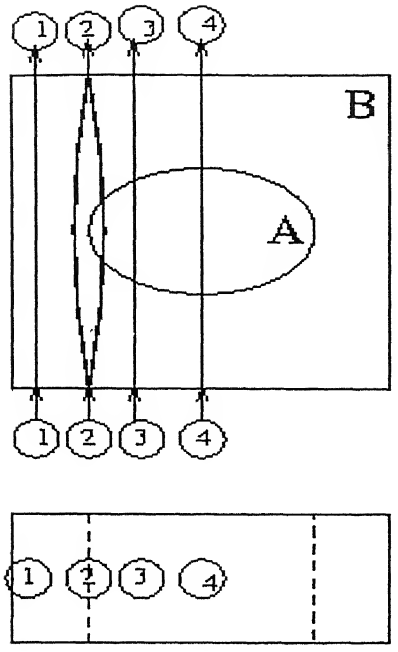

Fig. 4.3(a) Sample-6 of Nylon (B) with 30mm×20mm elliptical insertion of Epoxy Resin (A) with four positions of data collection

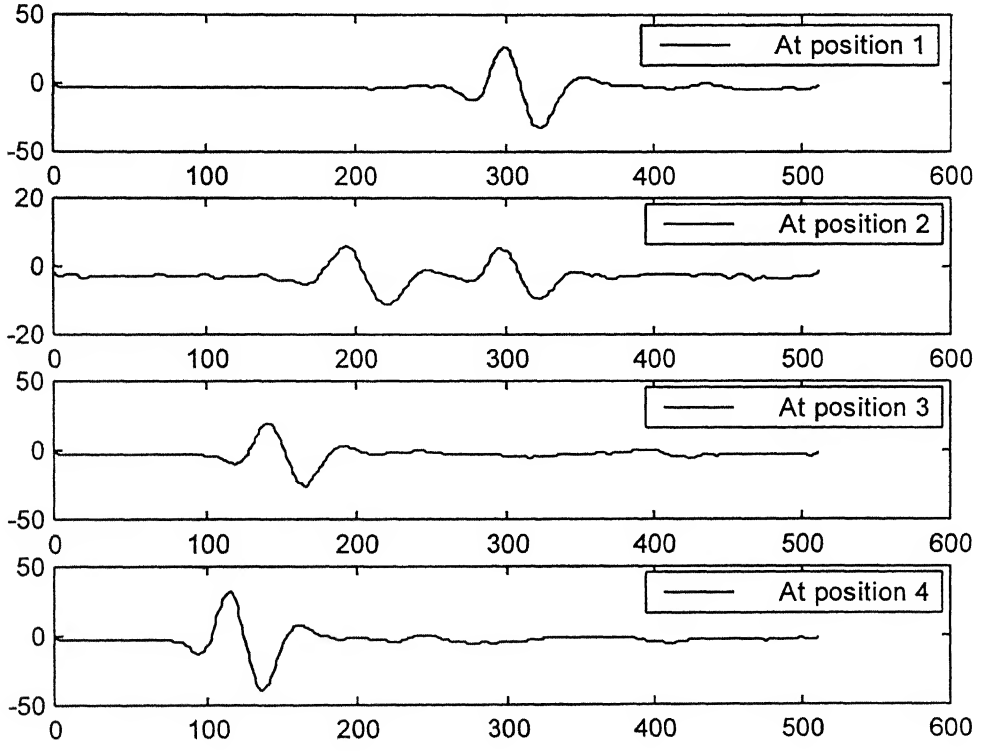

Fig. 4.3(b) Signals at four different positions (i.e. shown in fig. 4.3(a)) for Nylon sample with Epoxy resin elliptical insertion

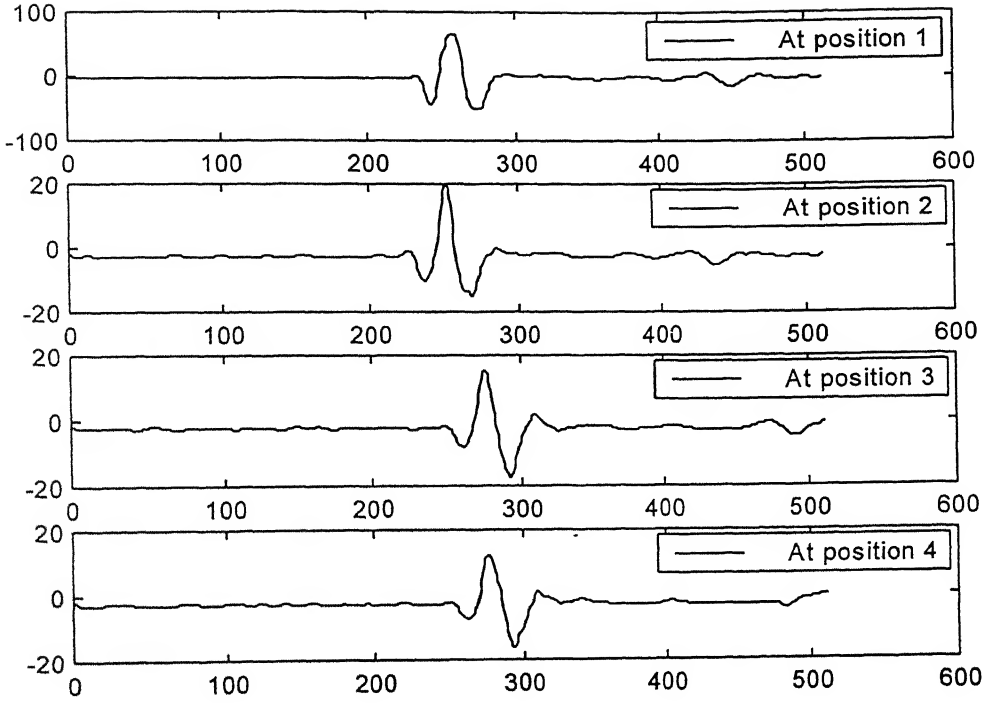

Fig. 4.3(c) Signals at four different positions (i.e. shown in fig. 4.3(a)) for Perspex sample with Epoxy resin elliptical insertion.

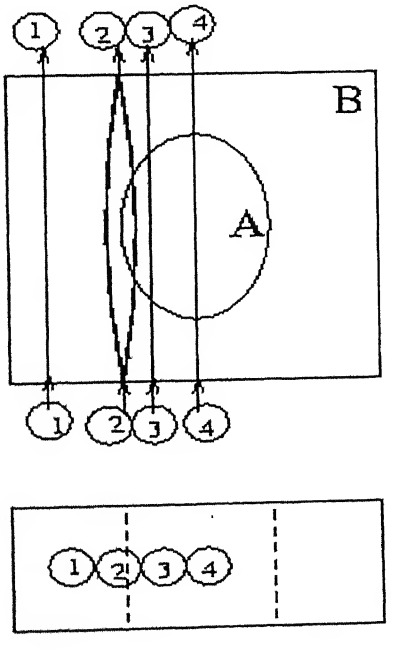

Fig. 4.4(a) Sample-6 of Nylon (B) with 30mm×20mm elliptical insertion of Epoxy Resin (A) with four positions of data collection when rays passing through the (B) sample at 90^0

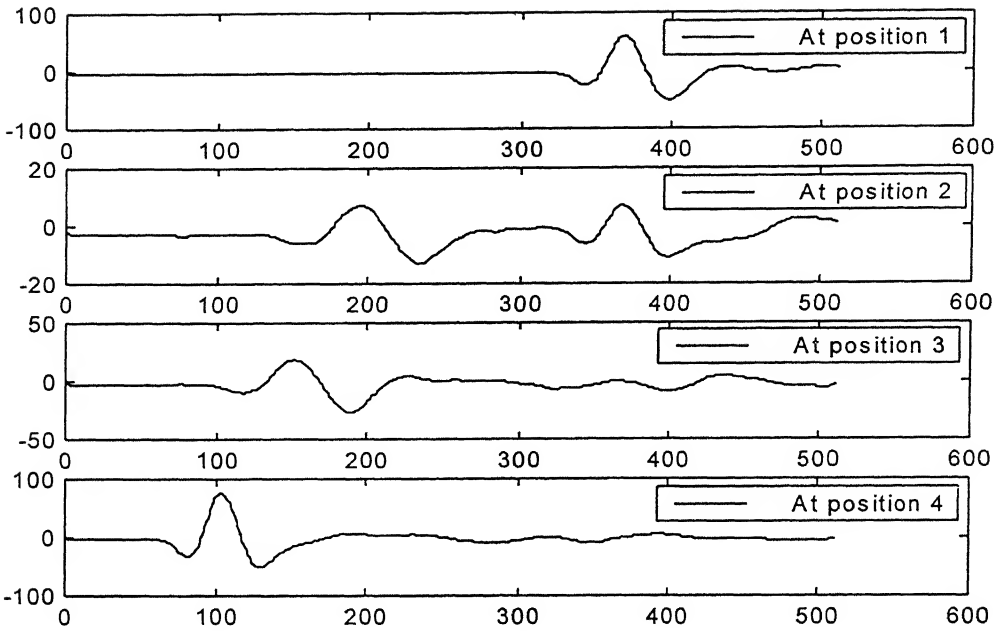

Fig. 4.4(b) Signals at four different positions (i.e. shown in fig. 4.4(a)) for Nylon sample with Epoxy resin elliptical insertion.

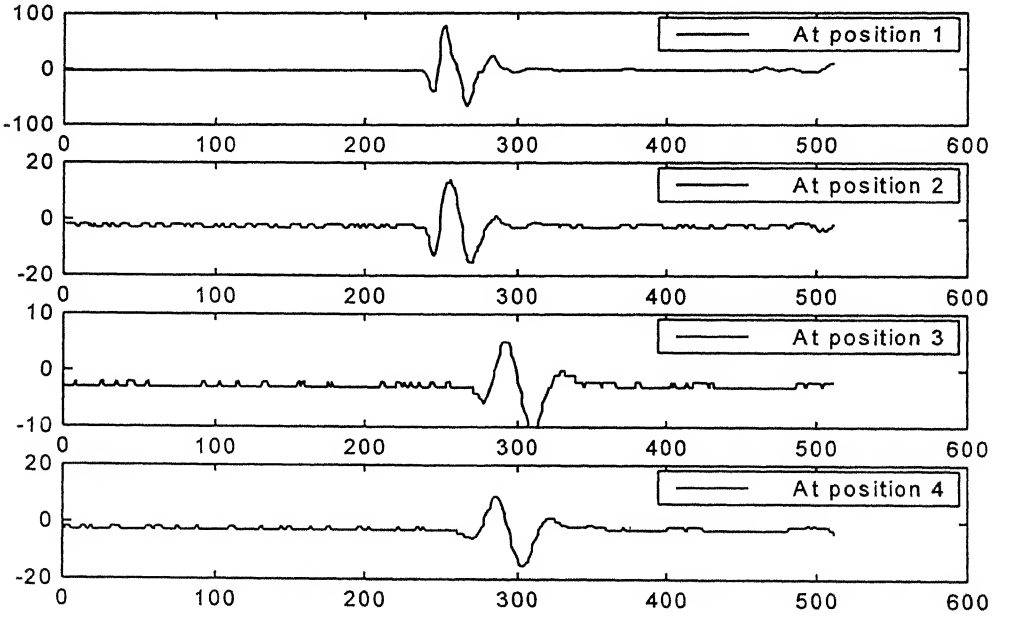

Fig. 4.4(c) Signals at four different positions (i.e. shown in fig. 4.4(a)) for Perspex sample with Epoxy resin elliptical insertion.

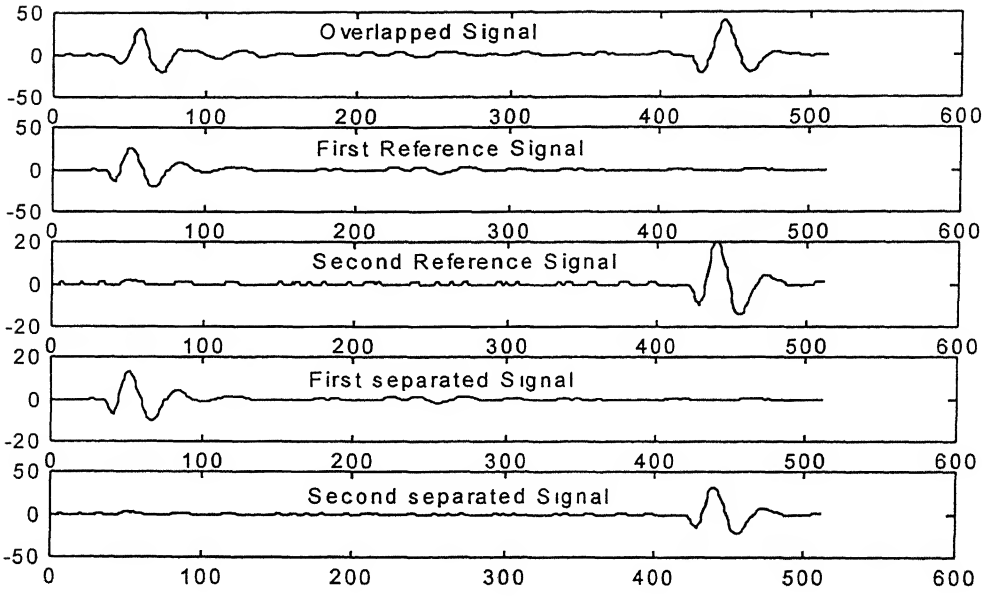

Fig. 4.5 Separation of Overlapped Signal with two Reference signal using least square method for Perspex sample with Aluminium rectangular insertion (20mm× 20mm)

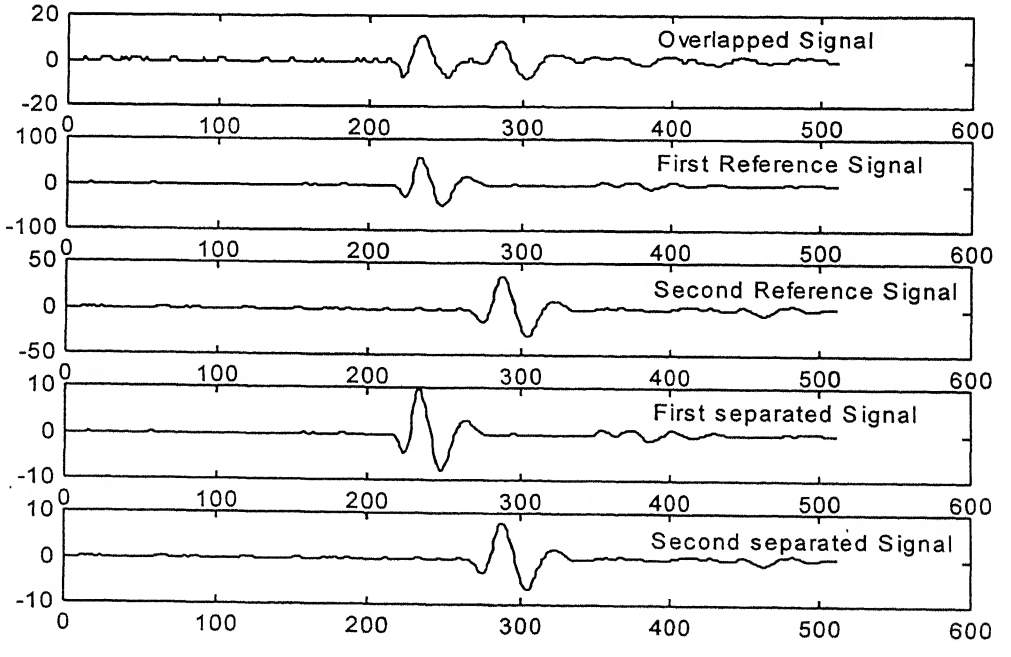

Fig. 4.6 Separation of Overlapped Signal with two Reference signal using least squares method for Perspex sample with Epoxy resin rectangular insertion (20mm× 20mm)

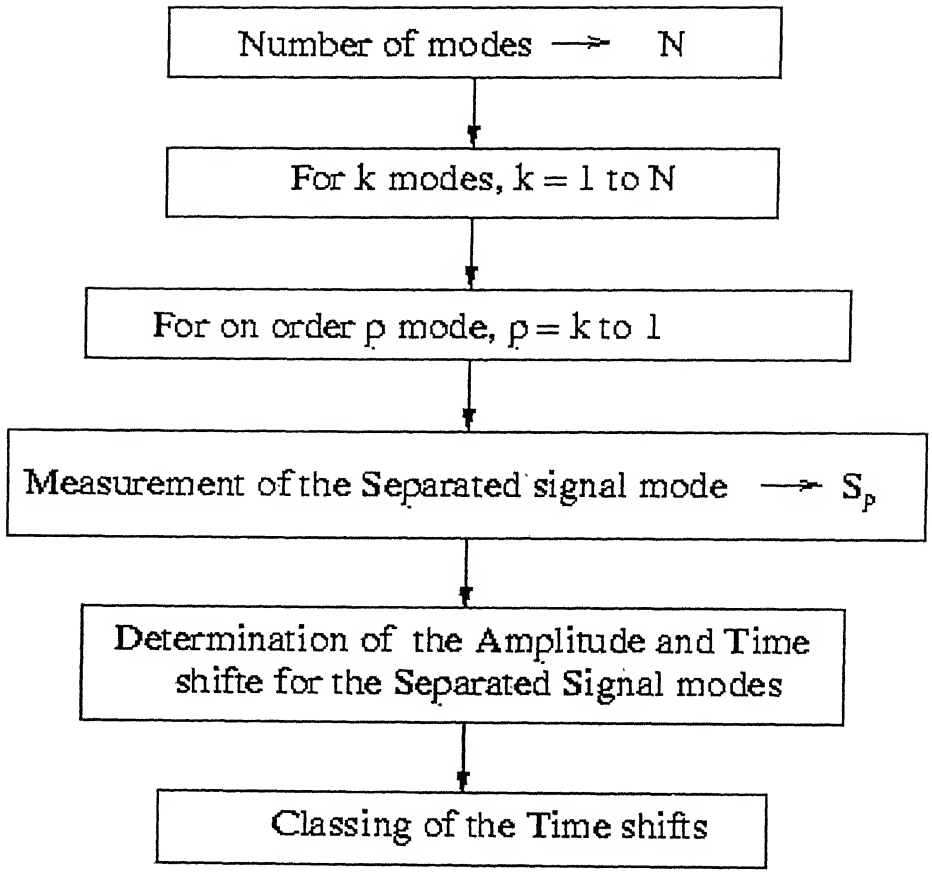

Where,

Separated signal mode, $S_p(\nu) = S(\nu) - R(\nu).\sum_{\substack{i=1 \\ i \neq p}}^{i=N} A_i.\exp(-2i\pi\tau_i\nu)$

Amplitude, $A_p = \sqrt{\dfrac{\int_{\nu_1}^{\nu_2} |S_p(\nu)|^2 \, d\nu}{\int_{\nu_1}^{\nu_2} |R(\nu)|^2 \, d\nu}}$, and

Time shift, $\tau_p = pos\left[\max\left(IFFT\left[S_p(\nu).R(\nu)\right]\right)\right]$

Fig 4.7. Flow chart for the mode separation algorithm of a signal with linear superposition of temporarily shifted reference signal

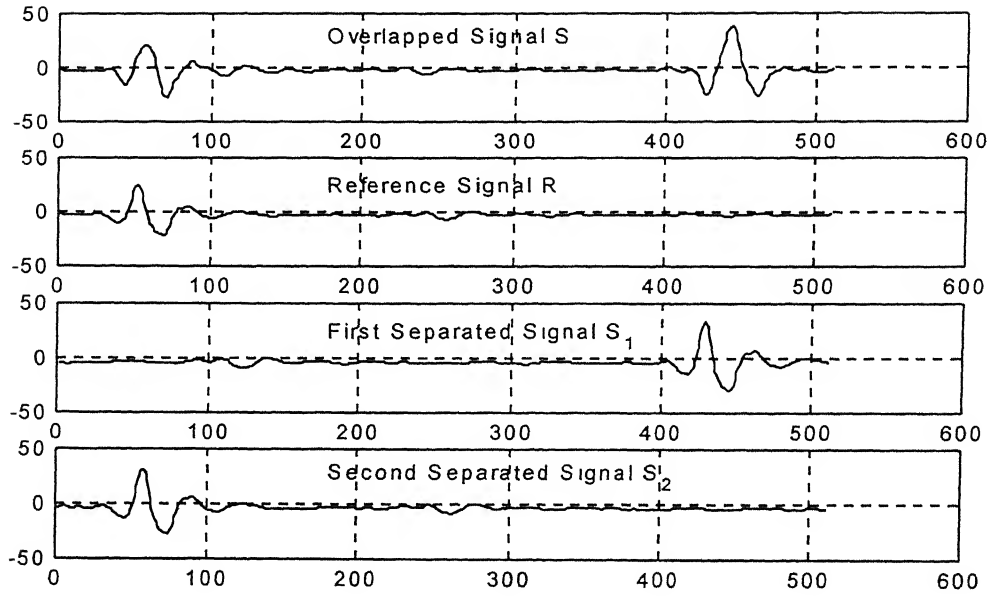

Fig 4.8. Separation of Overlapped Signal with a Reference signal using cross correlation method for Perspex sample with Aluminium rectangular insertion (20mm × 20mm)

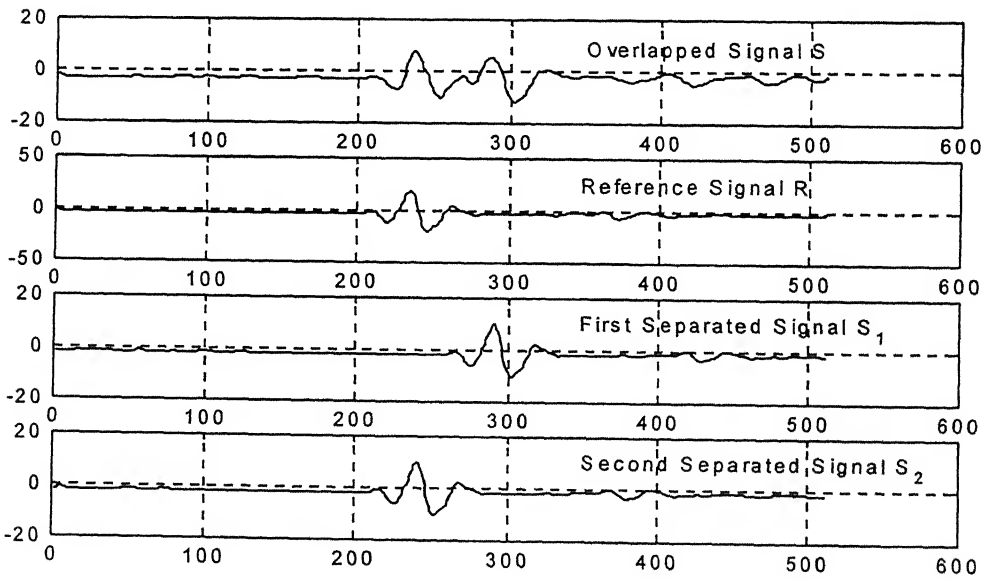

Fig 4.9. Separation of Overlapped Signal with a Reference signal using cross correlation method for Perspex sample with Epoxy resin rectangular insertion (20mm × 20mm)

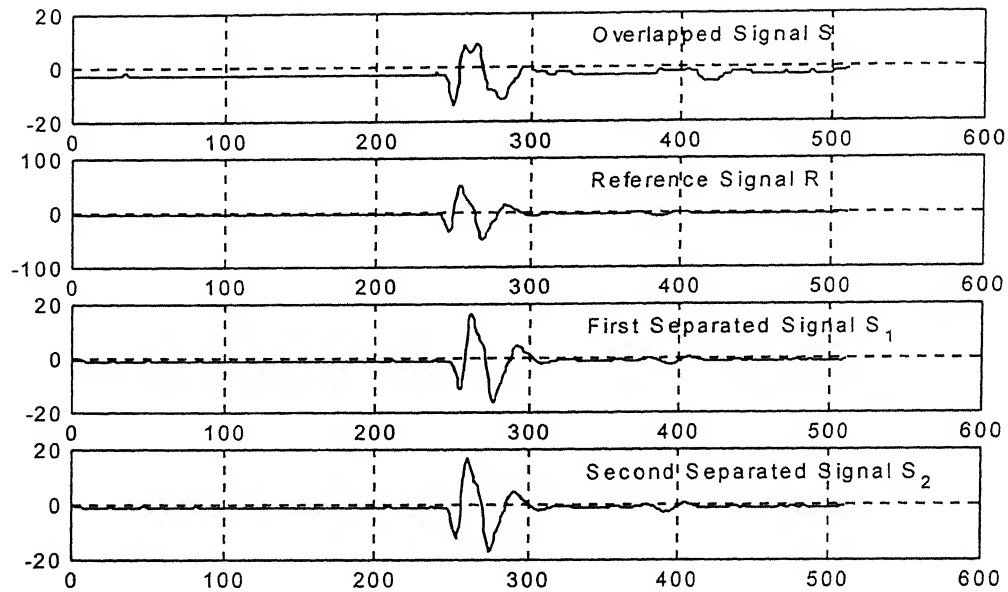

Fig 4.10. Separation of Overlapped Signal with a Reference signal using cross correlation method for Nylon sample with Epoxy resin rectangular insertion (20mm× 10mm)

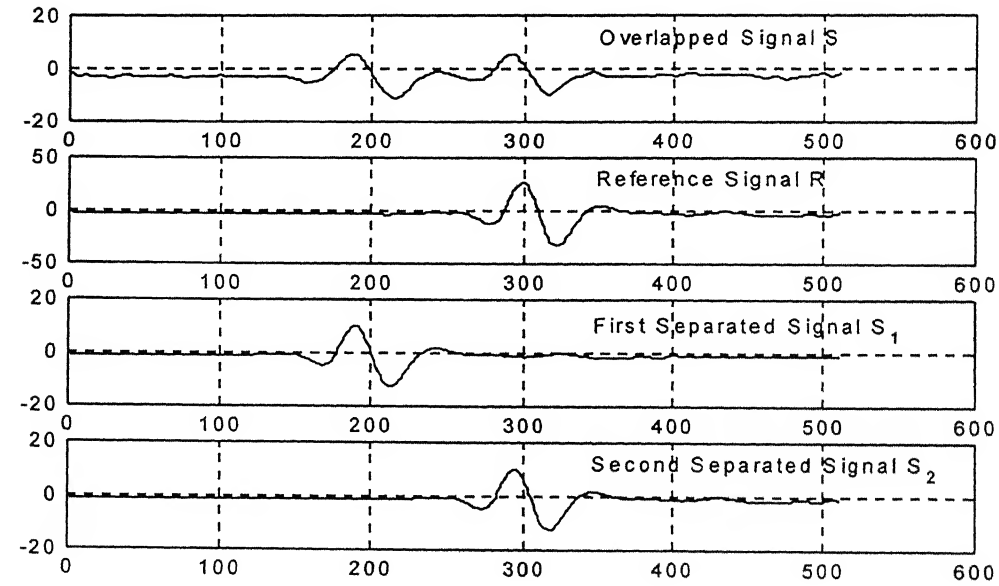

Fig 4.11. Separation of Overlapped Signal with a Reference signal using cross correlation method for Nylon sample with Epoxy resin elliptical insertion of 30mm major diameter and 20mm minor diameter, at insertion border

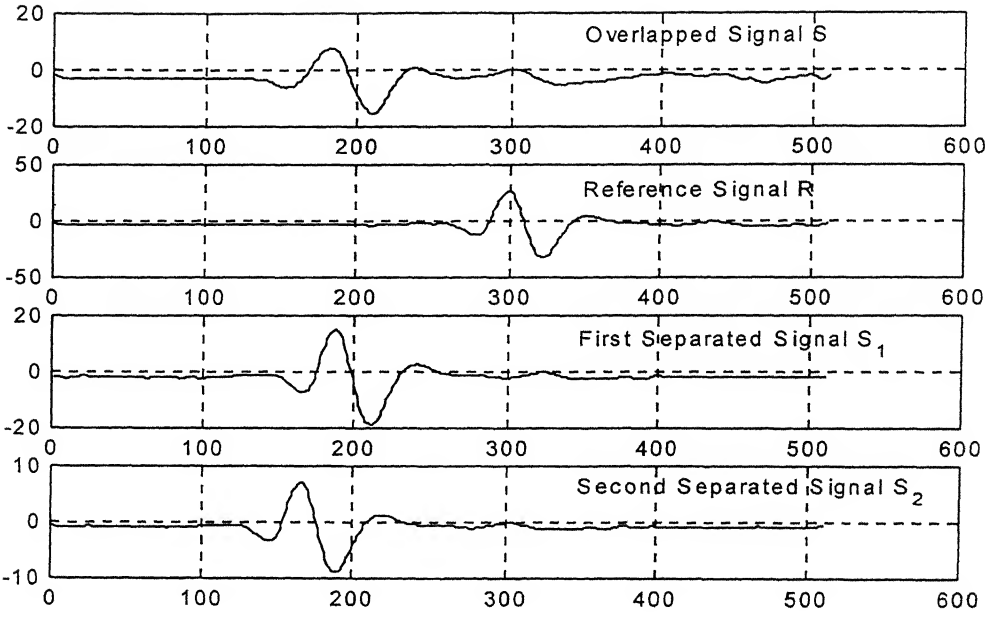

Fig 4.12. Separation of Overlapped Signal with a Reference signal using cross correlation method for Nylon sample with Epoxy resin elliptical insertion of 30mm major diameter and 20mm minor diameter, at 2mm inside of insertion

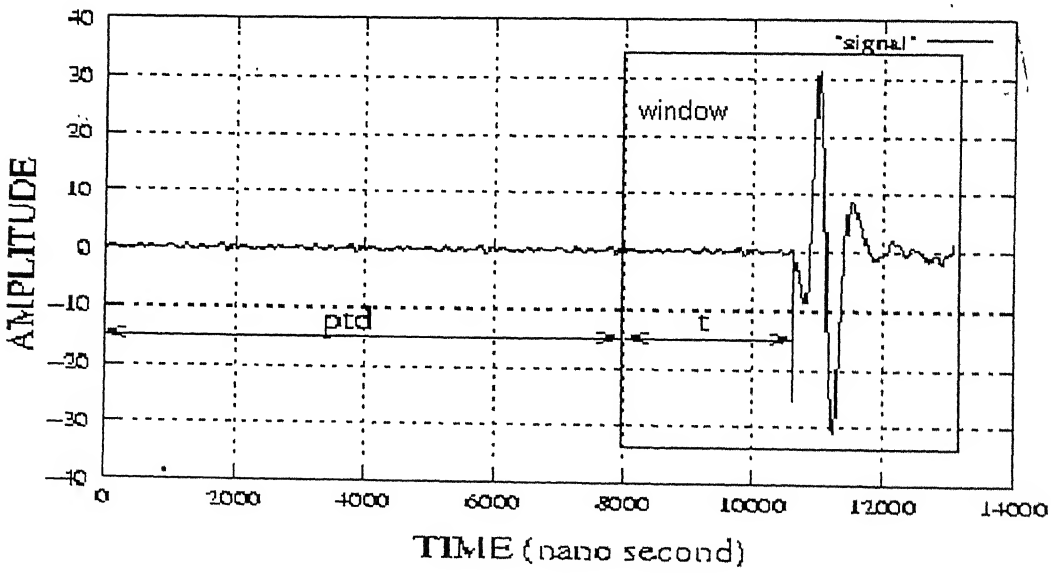

Fig 4.13. Time-delay (t) and post trigger delay (ptd) measurements for the Time of Flight (TOF) data from the signal (Time v/s Amplitude)

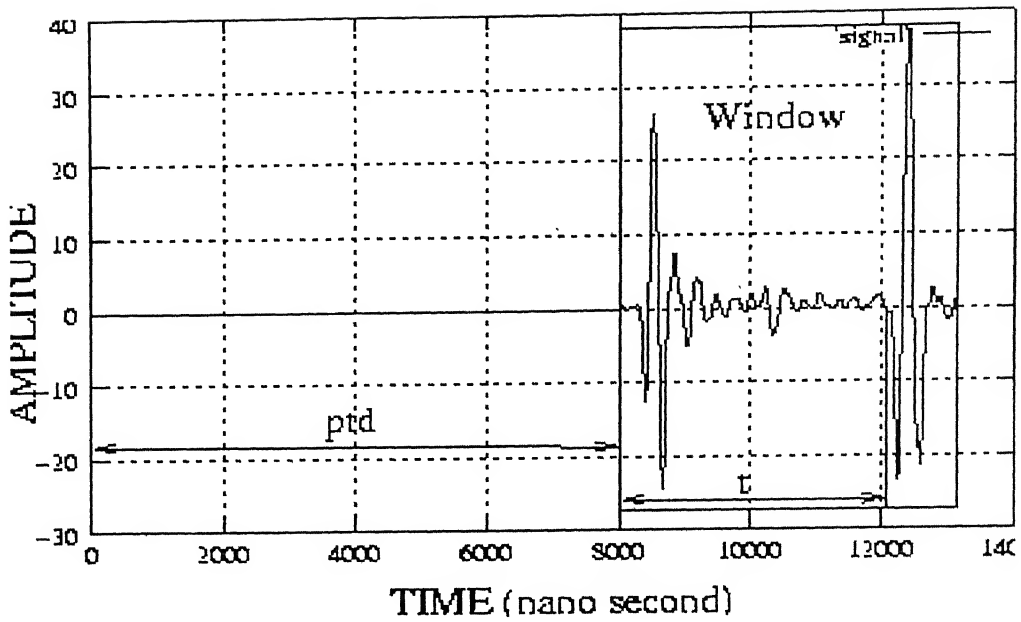

Fig 4.14. Time-delay (t) and post trigger delay (ptd) measurements for the Time of Flight (TOF) estimation from an overlapped signal, when wave velocity in insert material is slower than in base material.

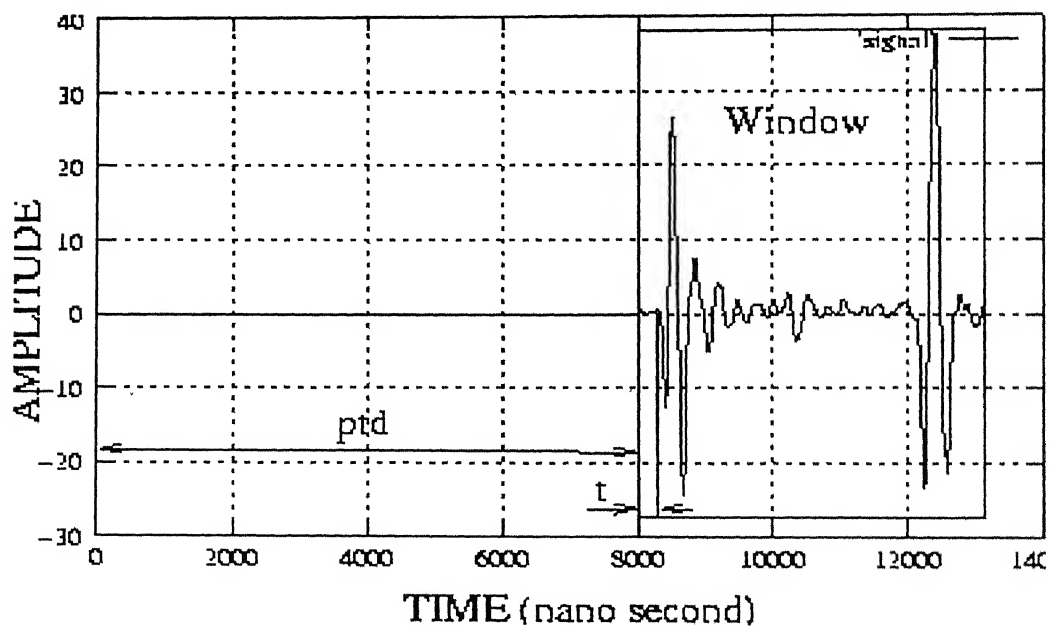

Fig 4.15. Time-delay (t) and post trigger delay (ptd) measurements for the Time of Flight (TOF) estimation from an overlapped signal of sample, when wave velocity in insert material is faster than in base material.

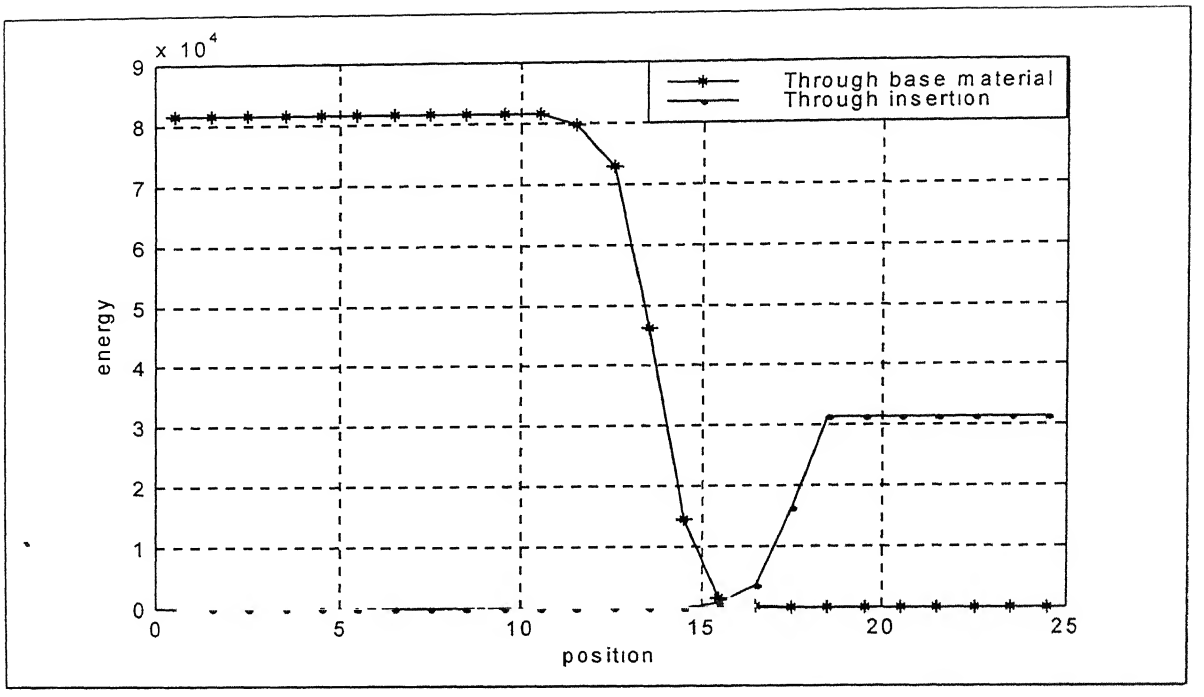

Fig 4.16. Energy of signals through base-material and through insertion verses various positions from one of the edges to center of the insertion for Perspex sample with Epoxy resin rectangular insertion of 20mm × 20mm

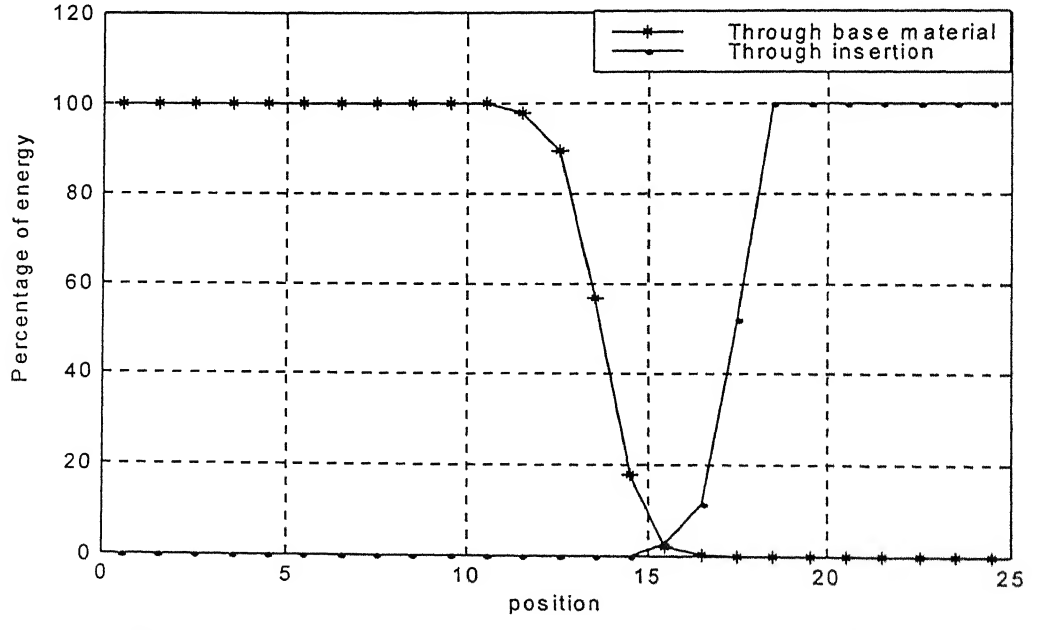

Fig 4. 17. Percentage of Energy (i.e. Normalized Energy) of signals through base-material and through insertion verses various positions from one of the edges to center of the insertion for Epoxy sample with Epoxy resin rectangular insertion of 20mm × 20mm

Chapter 5

ULTRASONIC TOMOGRAPHIC RECONSTRUCTION

5.1 INTRODUCTION

Computerized Tomography (CT) is widely used in large number of scientific, medical and technical fields. In conventional projection radiography, the result is obtained just in the form of a shadowgarph requiring a good interpretation. CT, however, uses tomographic reconstruction to combine the information from multiple projections. Thus, the CT information is displayed quantitatively as a reconstructed slice plane of the object and it can provide accurate quantitative measures of material characteristics in small volume of the component.

Although Computer Tomography was conceived originally for X-rays, in recent times, CT has been implemented successfully for other energy sources such as ultrasonic, laser, magnetic etc. Among these, Ultrasonic Tomography (UT) has special importance in application to Non Destructive Evaluation (NDE). Ultrasonic tomography can be defined as a technique to determine values of a spatially varying acoustic parameter of interest across a slice through an object.

5.2 RECONSTRUCTION TECHNIQUES

Reconstruction techniques are broadly classified into two groups:

1. Transformation methods or direct methods.
2. Series expansion methods.

Direct methods include direct algebraic methods and Fourier Transform methods and series expansion methods include Algebraic Reconstruction Technique (ART), Multiplicative Algebraic Reconstruction Technique (MART), Simultaneous Iterative Reconstruction Technique (SIRT), Entropy Optimization etc. ART and MART are further classified into different classes depending upon the way corrections are applied to the algorithms, are described below.

5.2.1 ART

The iterative process starts from an initial approximation of slowness (reciprocal of the velocity) s^0 and the current iterate s^k is corrected to a new iterate s^{k+1} by taking into account only a single ray, say i^{th}, and changing only the image values of the pixels which intersect this ray. The discrepancy between the measurement of TOF, τ_i and the pseudo-projection data $\bar{\tau}_i (= \sum_{j=1}^{N} w_{ij} \bar{s}_j^k)$ obtained from the current image s^k is redistributed among the pixels along the i^{th} ray proportionally to their weights w_{ij} (i.e. intercept of the i^{th} ray in the j^{th} pixel) in the whole ray. In this way, the pixel values along the i^{th} ray are corrected to conform to the i^{th} measurement without changing the rest of the image. The whole process may be expressed as

$$s^{k+1} = s^k + \frac{\tau_i - < w^i, s^k >}{\| w^i \|^2} w^i \tag{5.1}$$

where,

$$< w^i, s^k > = \sum_{j=1}^{N} w_{ij} s_j^k \tag{5.2}$$

$$w^i = \sum_{j=1}^{N} w_{ij} \tag{5.3}$$

and

$$\left\| w^i \right\|^2 = < w^i, w^i > \tag{5.4}$$

Introducing the relaxation parameter, the modified step for updating the iterate can be expressed as

$$s^{k+1} = s^k + \lambda \frac{\tau_i - < w^i, s^k >}{\| w^i \|^2} w^i \tag{5.5}$$

where, λ is the relaxation parameter, which is the real number, usually confined to the interval.

$$\varepsilon_1 \le \lambda \le 2 - \varepsilon_2, \qquad \varepsilon_1 \varepsilon_2 > 0 \tag{5.6}$$

If the correction in negative, it may happen that the calculated field of a reconstructed image negative, in which case it is set to zero, as discussed by *Gordon*.

ART may be further classified in different categories depending upon the correction applied. The four forms of ART are mentioned below. For all these algorithms, let s_j for j=1,2...N be the initial approximation of field value or pixel value. Where N is the total no of pixels.

Four classes of ART are

1. Mayinger ART
2. Gordon ART
3. Gilbert ART
4. Anderson ART

5.2.2 MART

When the correction is multiplicative, the ART is called Multiplicative ART (MART). While in MART, at each iteration, a new estimate of field value is calculated by multiplication of previous value and a correction term, i.e.

$$s_j^{k+1} = C \times s_j^k \qquad j = 1,2,.....N . \tag{5.7}$$

where C is correction term, s_j is the slowness value of the j^{th} pixel and k is the iteration number. Depending up on the correction term, the MART may be further classified in four classes. Algorithm remains the same for all but correction term varies. Algorithm of MART may be stated as follows

For each iteration k

Step 1: For each ray i, calculate the approximation TOF τ_i

$$\tilde{\tau}_i = \sum_{j=1}^{N} w_{ij} \tilde{s}_j \tag{5.8}$$

Step 2: Modify the value of j^{th} pixel, for all j=1,2...N, as

$$s_j^k = C \times s_j^{k-1} \tag{5.9}$$

Step 3: Repeat steps 1 and 2 for all rays. This completes the k^{th} iteration.

Step 4: Repeat steps 1 to 3 until

$$\frac{\tilde{s}^{k+1} - \tilde{s}^{k}}{\tilde{s}^{k}} \times 100 \leq e \tag{5.10}$$

where e is the stopping criteria, generally take it as error.

Four classes of MART are

1) GBH MART
2) GH MART
3) Lent MART
4) Lent2 MART

5.2.2.1 GBH MART

Gordon, Bender, and Herman (GBH) first proposed a MART algorithm for CT applications. Like all MART algorithms, it is an iterative technique. In this method the correction term is given by

$$C = \begin{cases} 1 - \dfrac{\lambda}{(w_{ij})_{\max}} \left(1 - \dfrac{\tau_i}{\tilde{\tau}_i} \right) & if\ \tilde{\tau}_i \neq 0, and w_{ij} \neq 0 \\ 1 & else \end{cases} \tag{5.11}$$

where,

λ is Relaxation parameter,

w_{ij}, is the Weight, intercept length in the j^{th} pixel with i^{th} ray,

$(w_{ij})_{\max}$, is the maximum of all weights on the i^{th} ray,

$\tau_i, \tilde{\tau}_i$, are measured and calculated projection data (TOF) respectively.

5.2.2.2 GH MART

This MART algorithm was proposed by *Gordon and Herman* (GH), with a slight and important modification of the GBH algorithm. The correction term is given by,

$$C = \begin{cases} 1 - \dfrac{\lambda w_{ij}}{(w_{ij})_{\max}} \left(1 - \dfrac{\tau_i}{\tilde{\tau}_i} \right) & if\ \tilde{\tau}_i \neq 0, and w_{ij} \neq 0 \\ 1 & else \end{cases} \tag{5.12}$$

5.2.2.3 Lent MART

Lent has proposed another multiplicative updating scheme, in which the correction term is computed as,

$$C = \begin{cases} \left(\dfrac{\tau_i}{\tilde{\tau}_i} \right)^{\lambda w_{ij}} & if\ \tilde{\tau}_i \neq 0, \\ 1 & else \end{cases} \tag{5.13}$$

5.2.2.4 Lent2 MART

A slight modification leads to Lent2 MART. The correction term is given by,

$$C = \begin{cases} \left(\dfrac{\tau_i}{\tilde{\tau}_i} \right)^{\lambda w_{ij}^*} & if\ \tilde{\tau}_i \neq 0, \\ 1 & else \end{cases} \tag{5.14}$$

where w_{ij}^* is given by $\dfrac{w_{ij}}{w_{\max}}$.

5.3 CONVERGENCE CRITERION

It is necessary to determine when an iterative algorithm has converged to a solution, which is optimal. In all algorithms, iterations are carried out until the following relation is satisfied,

$$\left|\frac{s^{k+1}-s^{k}}{s^{k}}\right|\times 100 \leq e \tag{5.15}$$

where, e is the stopping criterion. In the present work, e has been taken as 0.001. Here s^{k+1} is the slowness (field value) at $(k+1)^{th}$ iteration and s^{k} is the slowness at k^{th} iteration.

5.4 RESULTS AND DISCUSSION

In the present work, *Gordon and Herman (GH) MART* algorithm has been used for reconstruction of CT images, which essentially computes the slowness (inverse of velocity) distribution in the domain from numerous projections (TOF) data from each different view. In this work, ultrasonic waves travel through the sample (from a series of source locations) to receivers (detectors) at the opposite positions on the other side of the object in the *through transmission* method. In the Ultrasonic Computer Tomography (UCT), two types of approaches are using. They are straight-ray approach and curved-ray approach. In straight-ray approach the ray paths are assumed as straight lines. But, in the curved-ray approach ray-paths are assumed, with little bending. In the present work, simple straight-ray approach has been used.

The present study has been conducted on domains of various samples containing different inclusions as given in the following Table. 5.1.

Table 5.1

Sample Number	Material and Dimensions (All in mm)		Longitudinal wave Velocity (m/s)		Projection data type
	Base	Insert	Body	Insert	
1.	Perspex (50×50 Square)	Epoxy Resin (30×20 Ellipse)	2730	2650	4-view
2.	Perspex (50×50 Square)	Epoxy Resin (20×20 Square)	2730	2650	4-view
3.	Nylon (50×50 Square)	Epoxy Resin (30×20 Ellipse)	2300	2650	2-view

For reconstruction purpose the domain of each sample is divided into 50×50 grids (pixels, i.e. Cartesian grid of square picture elements) as shown in fig. 5.1(b). The pixels were numbered from 1 to 2500 (i.e. 50×50). While ultrasonic signal is passing through the material, the ray crosses various pixels. When the i^{th} ray is passing through the j^{th} pixel, the length of the intercept of the i^{th} ray in the j^{th} pixel is denoted by w_{ij}, called weight, as shown in fig. 5.1(a). In each view (of angle), the TOF data has been taken with 1mm of interval, called ray spacing. In 4-view projection, the analysis was repeated for four views (directions), namely 0^0, 90^0, 45^0 and 135^0, with respect to positive x-axis as shown in figs. 5.1(c) through 5.1(f). But, in case of 2-view reconstruction, the data has been considered for 0^0 and 90^0 views only. In the present work, 50 rays have been considered for both 0^0 and 90^0, and in each view, 71 rays have been considered for both 45^0 and 135^0. In the present work, for getting the data for 45^0 and 135^0, some special setup was used as shown in fig. 2.2(h). The ray locations were so chosen that the ray spacing (perpendicular distance between rays) is uniform for all views (i.e. one pixel dimension, 1mm). TOF data has been computed for all rays, as discussed in the previous chapter.

The reconstruction was conducted from projection (TOF) data. Projections have been taken either from four views (directions) namely 0^0, 90^0, 45^0 and 135^0 (in case of 4-view projection) or from two views (directions) namely 0^0 and 90^0 (in case of 2-view projection). The details of each view are discussed below.

1. Ray-paths along 0^0 direction (x-axis)

In this view, in all 50 data have been collected from 50 ray-paths, each ray originating from a pixel in the first column (fig. 5.1(c)) of the grid and being excited parallel to x-axis. In this case first ray-path has been taken at 0.5mm (approximately) distance from x-axis and parallel to x-axis. The other rays have been passed parallel to the x-axis with uniform ray spacing, being equal to unit pixel length (i.e. 1mm). The corresponding receiver to any receiver to any source, in this case, was situated exactly opposite it in the x-direction, as shown in fig. 5.1(c).

2. Ray-paths along 90^0 direction (x-axis)

As explained earlier, in this view also 50ray-paths have been taken into consideration. In this case, each ray originating from every column of the grid, towards y-direction as shown in fig. 5.1(d). In this case also the ray spacing (i.e. 1mm) is constant and is same as that in case of 0^0 view.

3. Ray-paths along 45^0 direction

In this case, 71ray-paths have been considered. In this case also the ray spacing is uniform and is equal to 1mm. But, for getting TOF data, some special setup has been used as shown in fig. 2.2(h), by using four right-angle triangular Perspex (same as base material of the specimen) pieces. The time of flight was taken for this extra material, has been subtracted from the experimental TOF data for the getting input projection (TOF) data.

4. Ray-paths along 135^0 direction

As before, 71 ray-paths have been considered in this view as shown in fig. 5.1(f), with ray spacing of 1mm (same as above cases).

In all these cases, some water gaps (approximately 1mm each) were maintained between source probe and specimen plate surface, and between specimen plate surface and detector probe, for free movement of the probes. The time of flight for the signal through these gaps were taken into recount in analysis the experimental TOF data.

5.5 IMAGE RECONSTRUCTION

In the present work of Ultrasonic Computer Tomography (UCT), a total of 242 projection data are available for 4-view reconstruction, where as 100 data are available for 2-view reconstruction. The reconstruction algorithm here determines the slowness value of each pixel.

The relation between the TOF, slowness and weight (intercept length) matrix is given by.

$$[W]\{S\} = \{\tau\} \tag{5.16}$$

where, W is the weight matrix, of 242 ray × 2500 pixels in case of 4-view reconstruction and 100 ray × 2500 pixels in case of 2-view reconstruction, S is slowness vector of 2500 pixels; and τ is the TOF vector of 242 ray-paths in case of 4-view and of 100 ray-paths in case of 2-view reconstruction.

The reconstruction procedure has been implemented in four steps.

1. In this first step, the algorithm determines the co-ordinates of the all pixels of the domain.
2. In this step the algorithm evaluates the weight matrix of 242 × 2500 (or) 100 × 2500 dimension, with help of first step results.
3. In this step, using weight matrix and projection data (Time of flight data), it finds the slowness vector using GH MART algorithm. In this program, the first iteration starts with initial guess pixel (slowness) values, other than zeros as, it is multiplicative algorithm. In this reconstruction algorithm, the pixel values are updates to bring in to better agreement with the measured projection. This updating of pixel values is continued until a stopping criterion is met, as shown in equation.5.10. A possible stopping criteria is the absolute incremental and the change is less than some prescribed value, the iteration process stopped.

4. Finally, the slowness values all pixels were changed to the values between 0 and 255 in PGM format to plot the reconstructed image.

In the present work, Normalized RMS Error (L2 error) has been used to find the deviation of reconstructed field from the exact field. The Normalized Root Mean Square Error (EL_2) is defined as

$$EL_2 = \frac{\sqrt{\frac{\sum_{i=1}^{N}(s_{i,a} - s_{i,r})^2}{N}}}{s_{\max} - s_{\min}} \times 100 \qquad (5.17)$$

where, $s_{i,a}$, $s_{i,r}$ are the actual and reconstructed slowness values of the i^{th} pixel respectively. N is total number of pixels. $s_{\max}$, $s_{\min}$ are maximum and minimum of all pixel values respectively. The actual slowness of the Perspex, Nylon and Epoxy resin have been taken as 366.3 $\mu s/m^2$, 434.8 $\mu s/m^2$ and 381.7 $\mu s/m^2$ respectively.

For all the samples, the convergence criterion has been taken as 0.001. The percentage of sound velocity difference between the base material and the insert material is less than 16% in all the samples, so straight-ray assumption is valid. In the present work, the effects of the relaxation parameter on the reconstruction accuracy and convergence rate have also been presented.

(i). Sample 1:

The sample is made of Perspex with rectangular insertion of Epoxy resin and has been tested with different relaxation parameters. Table 5.2 shows the Normalized RMS (EL_2) error and number of iterations till the convergence criterion is met at various relaxation parameters (λ). From these results, it has been found that, at relaxation parameter λ=0.35, it gives better accuracy of the reconstructed image (i.e. EL_2 error is minimum, 18.753%), with least number of iterations (i.e. 34). Datta [23] reported that 47.1% RMS error was the least at λ=1.0 for rectangular insertion sample with 4-view projection with FEM simulated data. Figs. 5.2(a) to 5.2(d) show the reconstructed image at four different relaxation parameters i.e. λ=0.02, 0.35, 0.5 and 1.8. The insert is also shown by a white line.

ii. Sample 2:

The sample is of Perspex as a base material with elliptical insertion of Epoxy resin. In this sample, the velocity of sound in insert material is slower than the base material. The accuracy of the reconstructed images in terms of Normalized RMS error (EL_2) and convergence rate has been tested at all different relaxation parameters (λ). Table. 5.3 shows the EL_2 error and the number of iterations at various relaxation parameters. It can be seen that at λ=0.316, the reconstructed image has minimum Normalized RMS error (i.e. 24.6722%) and least number of iterations (36). Figs. 5.3(a) to 5.3(d) show the reconstructed images at four different relaxation parameters, namely λ=0.05, 0.3, 0.316 and 1.5. It shows that the image for λ=0.316, has better appearance compared to the reconstructed images at other relaxation parameters. It has also been found that, the Normalized RMS error depends on the shape and the size of the defect, as the EL_2 error of the elliptical inserted sample is more than the rectangular inserted sample, even though both samples were tested with 4-view projection data.

iii. Sample 3:

In this case, the Nylon sample with elliptical Epoxy resin insertion has been tested with 2-view projection data, i.e. 0^0 and 90^0. The accuracies of the reconstructed images and convergence rates have been tested at various relaxation parameters. Table 5.4 shows the Normalized RMS (EL_2) error and iterations at different relaxation parameters. In this test, it has been found that, the normalized RMS error (i.e. 32.4328) is minimum at λ=1.0 with minimum number of iterations (i.e. 2). Figs. 5.4(a) to 5.4(d) show the reconstructed images at four relaxation parameters, i.e. λ=0.01, 0.1, 1.0 and 1.8.

From above tests for the three samples using the present method of TOF estimation the reconstruction seem to be better. It can also seen that, reconstruction from 4-view projection data gives the better results than 2-view reconstruction. And it has also been found that, at optimum relaxation parameter, the reconstruction gives more accurate

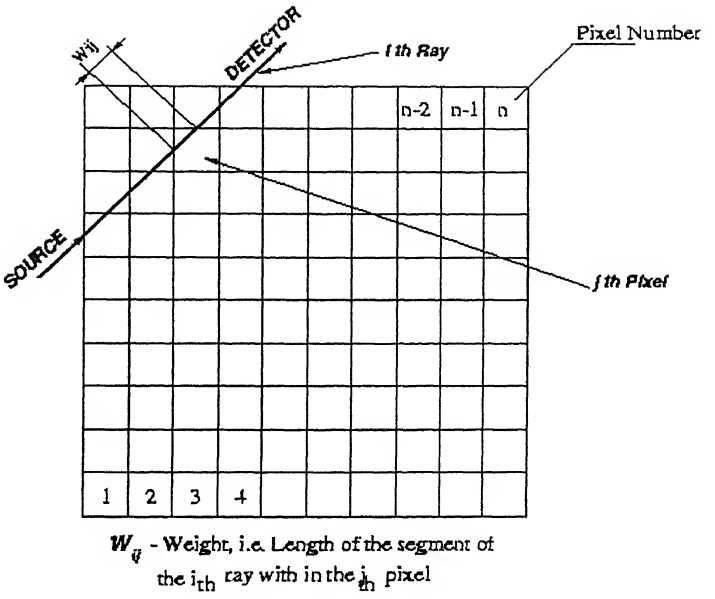

Fig. 5.1(a) Descretization of the object plane

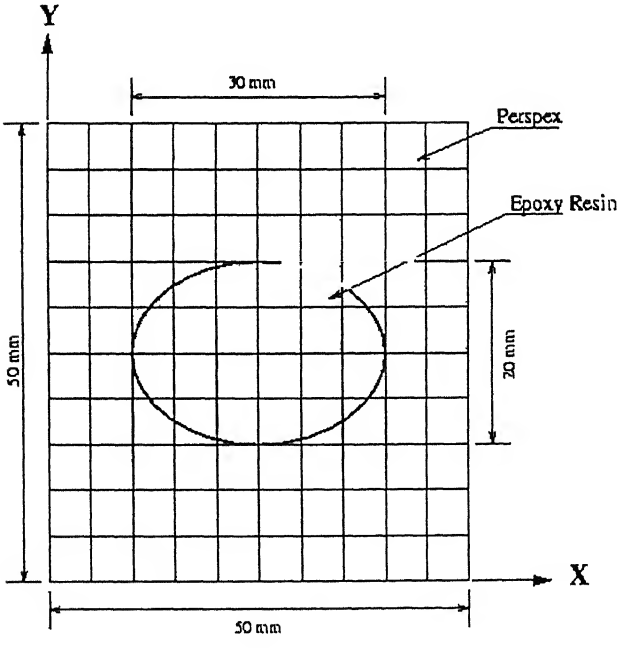

Fig. 5.1(b) Schematic view of the domain under consideration

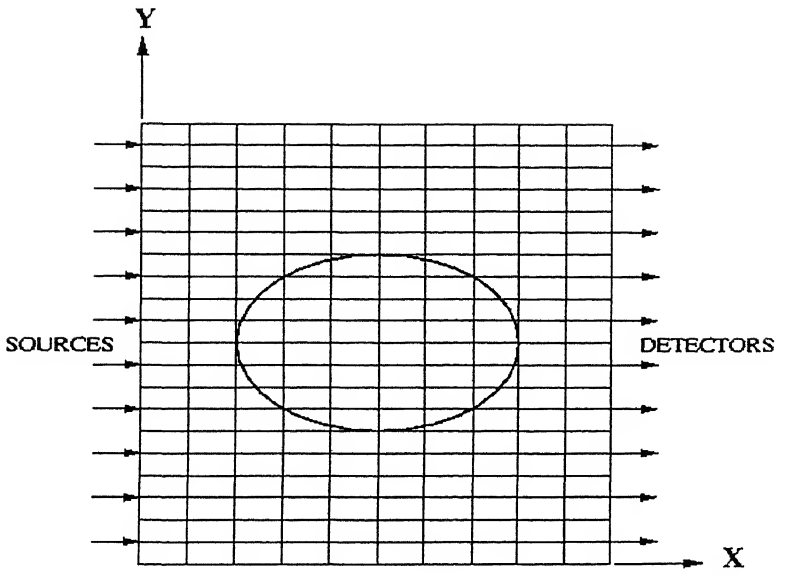

Fig. 5.1(c) Ray paths along 0^0 direction (x-direction)

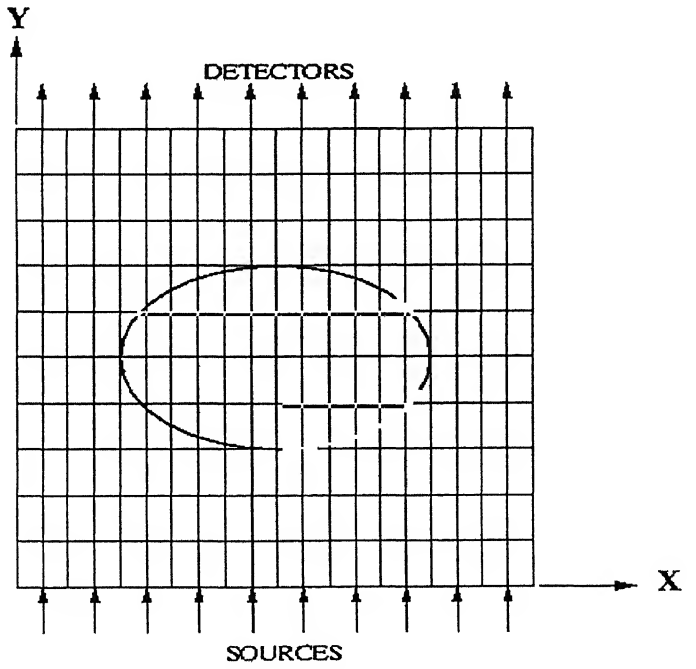

Fig. 5.1(d) Ray paths along 90^0 direction (y-direction)

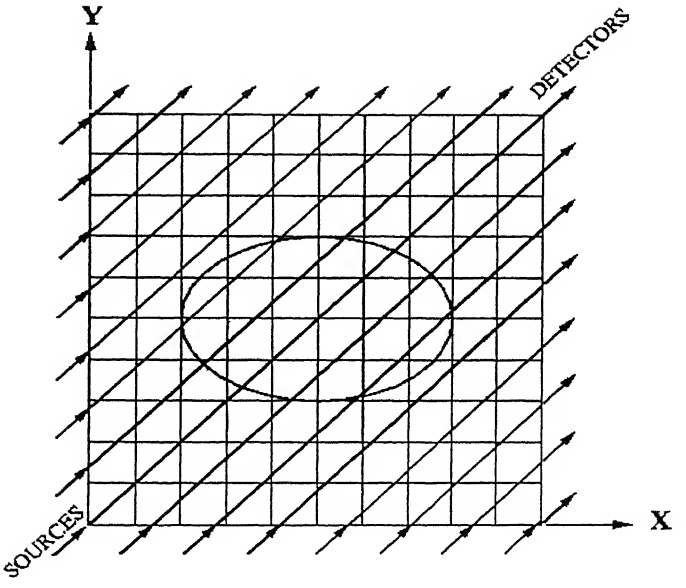

Fig. 5.1(e) Ray paths along 45^0 direction to x-axis

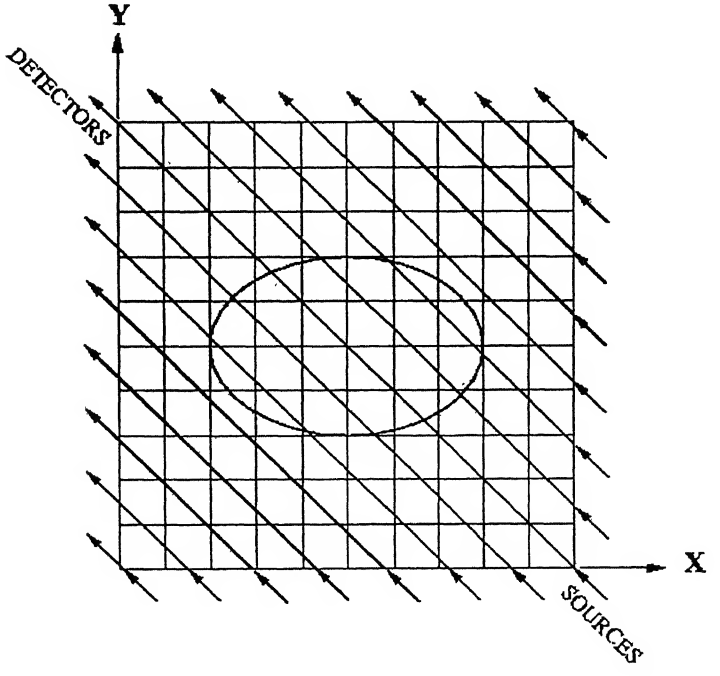

Fig. 5.1(f) Ray paths along 135^0 direction to x-axis

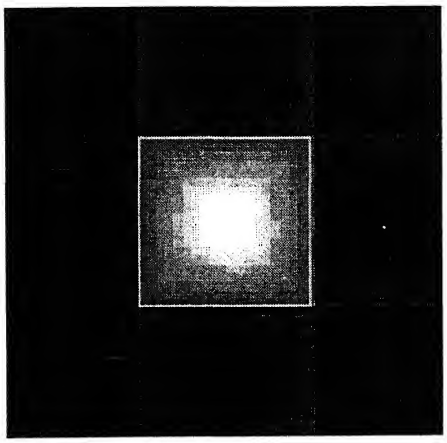

(a) $\lambda = 0.02$

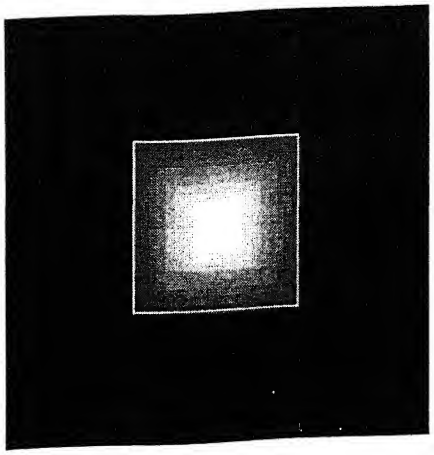

(b) $\lambda = 0.35$

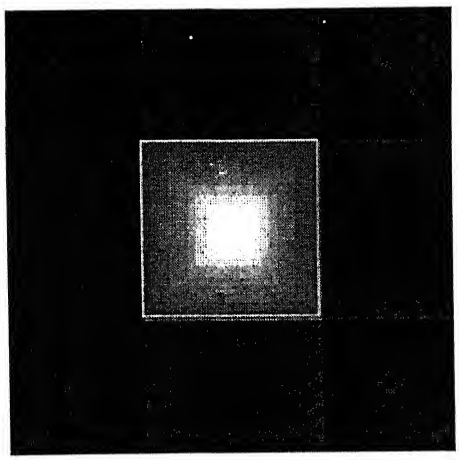

(c) $\lambda = 0.5$

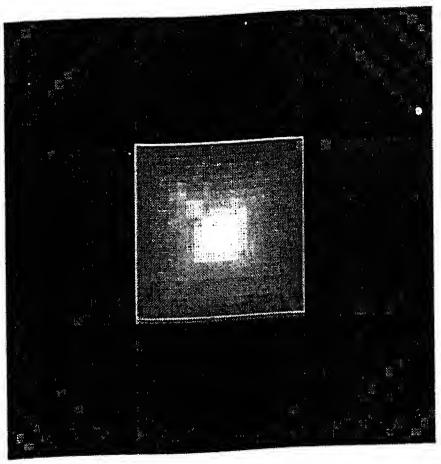

(d) $\lambda = 1.8$

Figs. 5.2(a-d) Tomographic reconstructed images from 4-view projection data for Rectangular Insertion with different relaxation parameters (λ) for Epoxy (slower material) inserted in the Perspex (faster material) sample.

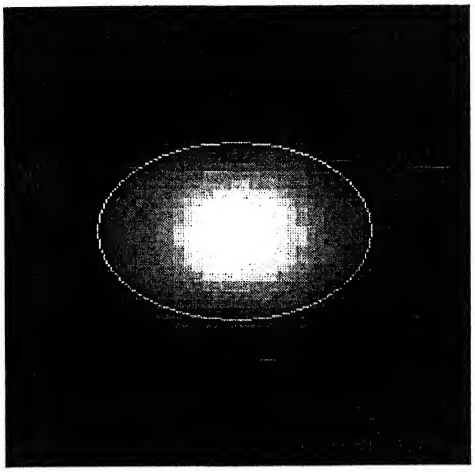

(a) $\lambda = 0.05$

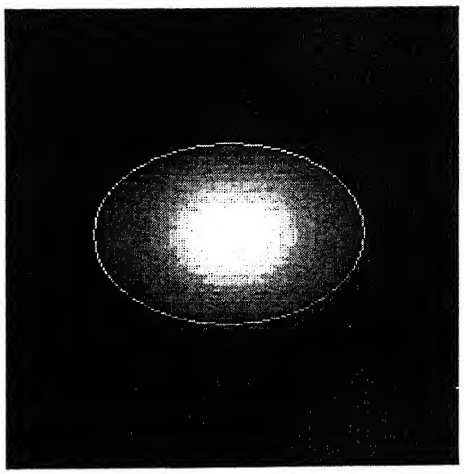

(b) $\lambda = 0.3$

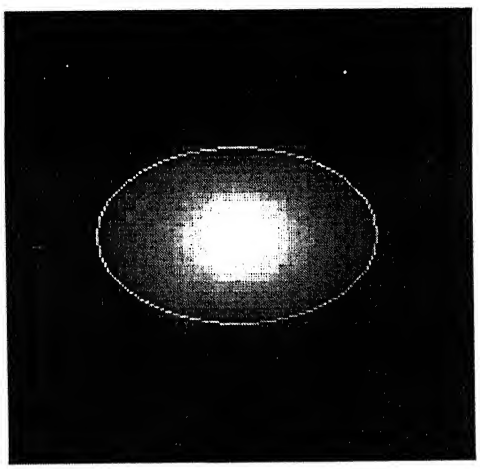

(c) $\lambda = 0.316$

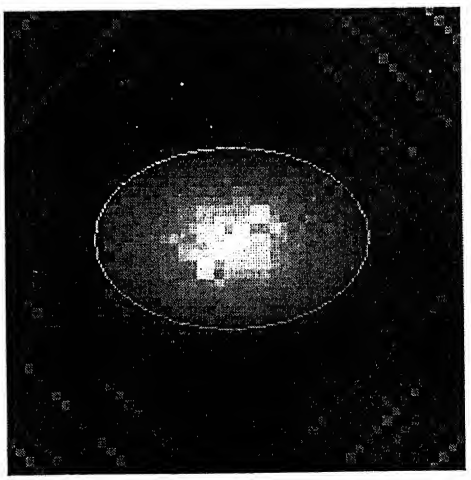

(d) $\lambda = 1.5$

Figs. 5.3 (a-d). Tomographic reconstructed images from 4-view projection data for Elliptical Insertion with different relaxation parameters (λ) for Epoxy (slower material) inserted in the Perspex (faster material) sample.

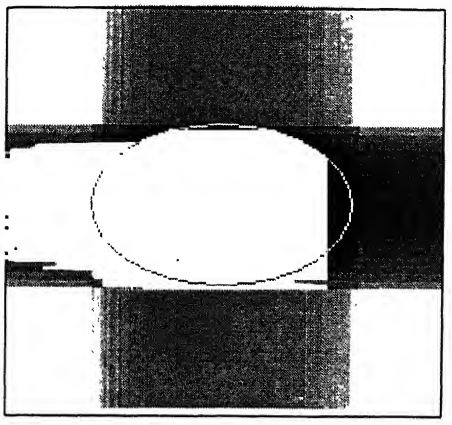

(a) $\lambda = 0.01$

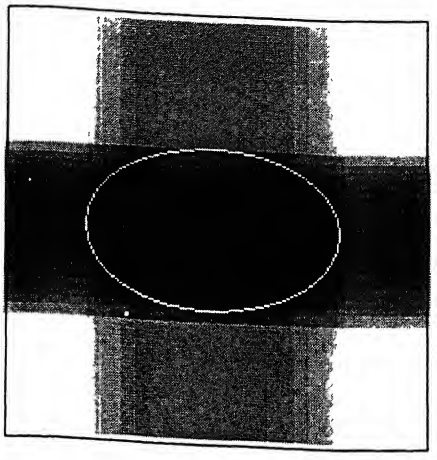

(b) $\lambda = 0.1$

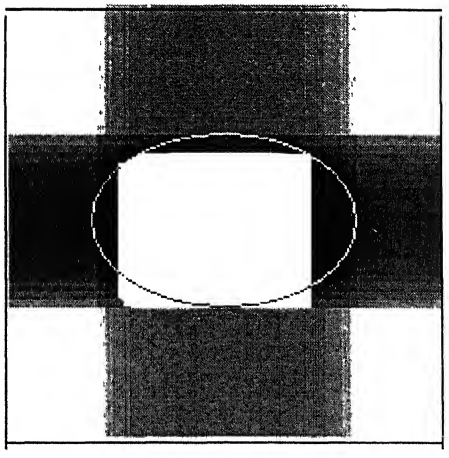

(c) $\lambda = 1.0$

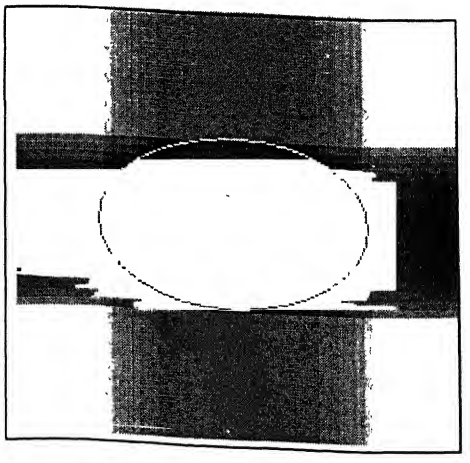

(d) $\lambda = 1.8$

Figs. 5.4 (a-d). Tomographic reconstructed images from 2-view projection data for Elliptical Insertion with different relaxation parameters (λ) for Epoxy (faster material) inserted in the Perspex (slower material) sample.

S. No.	Relaxation Parameter (λ)	Number of Iterations	Normalized RMS Error (EL2)
1	0.02	257	18.853
2	0.05	136	18.853
3	0.08	96	18.853
4	0.10	82	18.847
5	0.20	50	18.818
6	0.30	38	18.774
7	0.34	35	18.759
8	0.345	35	18.755
9	0.348	35	18.754
10	0.349	35	18.754
11	0.35	34	18.753
12	0.36	34	18.755
13	0.4	252	19.281
14	0.5	422	20.023
15	1.0	498	24.393
16	1.5	318	25.101
17	1.8	197	24.815

Table 5.2 Normalized RMS Error of the reconstructed images of the Rectangular Epoxy inserted Perspex sample from 4-view projection data with different relaxation parameters (λ)

S.No.	Relaxation Parameter (λ)	Number of Iterations	Normalized RMS Error (EL2)
1	0.05	125	24.87
2	0.08	88	24.85
3	0.1	74	24.8377
4	0.2	47	24.7746
5	0.3	37	24.6884
6	0.31	36	24.6792
7	0.311	36	24.6765
8	0.312	36	24.6757
9	0.313	36	24.6745
10	0.314	36	24.6741
11	0.315	36	24.6729
12	0.3155	36	24.6724
13	0.316	36	24.6722
14	0.317	36	24.6734
15	0.32	157	24.8908
16	0.35	283	25.1578
17	0.4	414	25.5147
18	0.5	534	26.05
19	1.0	541	27.41
20	1.5	355	28.248

Table 5.3 Normalized RMS Error of the reconstructed images of the Epoxy elliptical inserted Perspex sample from 4-view projection data with different relaxation parameters (λ)

S. No.	Relaxation Parameter (λ)	Number of Iterations	Normalized RMS Error (EL2)
1	0.01	438	32.407
2	0.02	254	32.419
3	0.05	119	32.423
4	0.08	79	32.423
5	0.1	65	32.423
6	0.5	14	32.433
7	0.8	7	32.4333
8	0.9	5	32.4333
9	0.95	5	32.4328
10	1.0	2	32.4328
11	1.05	5	32.4328
12	1.1	5	32.4328
13	1.2	7	32.4333
14	1.5	15	32.4333
15	1.8	46	32.42226

Table 5.4 Normalized RMS Error of the reconstructed images of the Epoxy elliptical inserted Nylon sample from 2-view projection data with different relaxation parameters (λ)

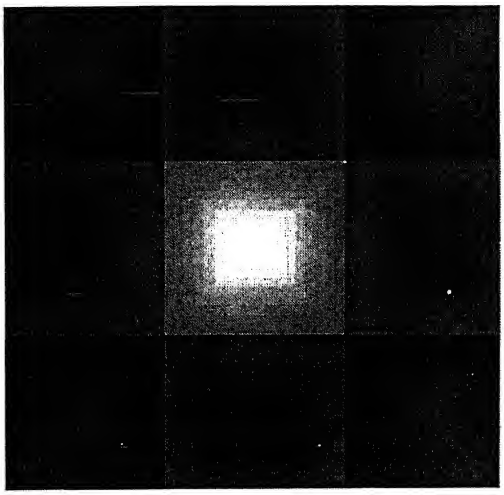

(a) $\lambda = 0.1$

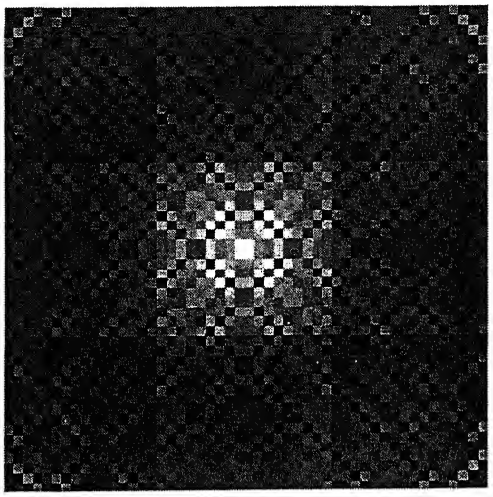

(b) $\lambda = 0.5$

Fig. 5.5 (a-b) Tomographic reconstructed images from 4-view projection data for Rectangular Insertion with different relaxation parameters (λ) for Epoxy (slower material) inserted in the Perspex (faster material) sample with out signal mode separation

S. No.	Relaxation Parameter (λ)	Number of Iterations	Normalized RMS Error (EL2)
1	0.1	92	21.307
2	0.5	538	36.842
3	1.0	967	38.644
4	1.5	1023	38.851

Table 5.5 Normalized RMS Error of the reconstructed images of the Rectangular Epoxy inserted Perspex sample from 4-view projection data with different relaxation parameters (λ) with out signal mode separation

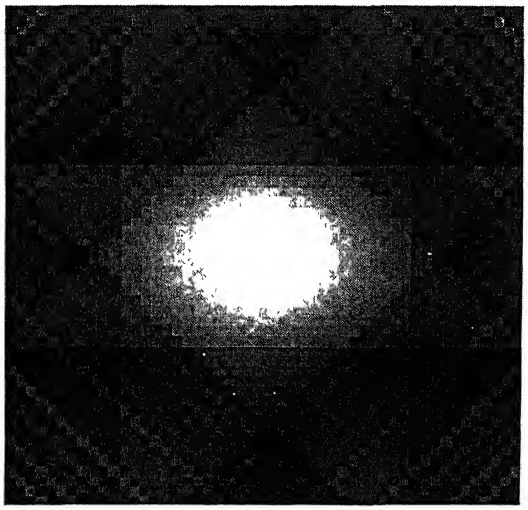

(a) $\lambda = 0.5$

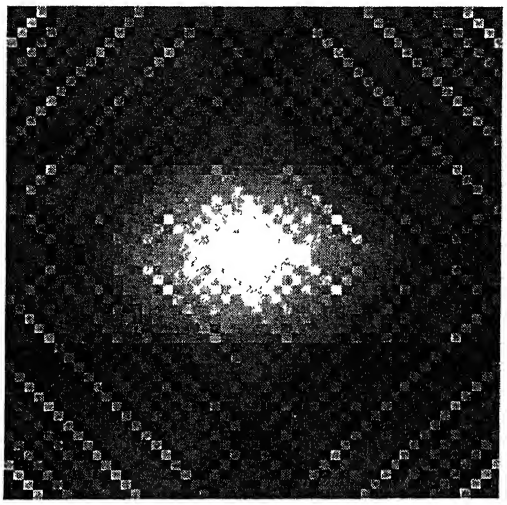

(b) $\lambda = 1.5$

Fig. 5.6 (a-b) Tomographic reconstructed images from 4-view projection data for Elliptical Insertion with different relaxation parameters (λ) for Epoxy (slower material) inserted in the Perspex (faster material) sample with out signal mode separation.

S. No.	Relaxation Parameter (λ)	Number of Iterations	Normalized RMS Error (EL2)
1	0.1	76	25.731
2	0.5	617	26.529
3	1.0	608	29.492
4	1.5	838	32.711

Table 5.6 Normalized RMS Error of the reconstructed images of the Epoxy elliptical inserted Perspex sample from 4-view projection data with different relaxation parameters (λ) with signal mode separation.

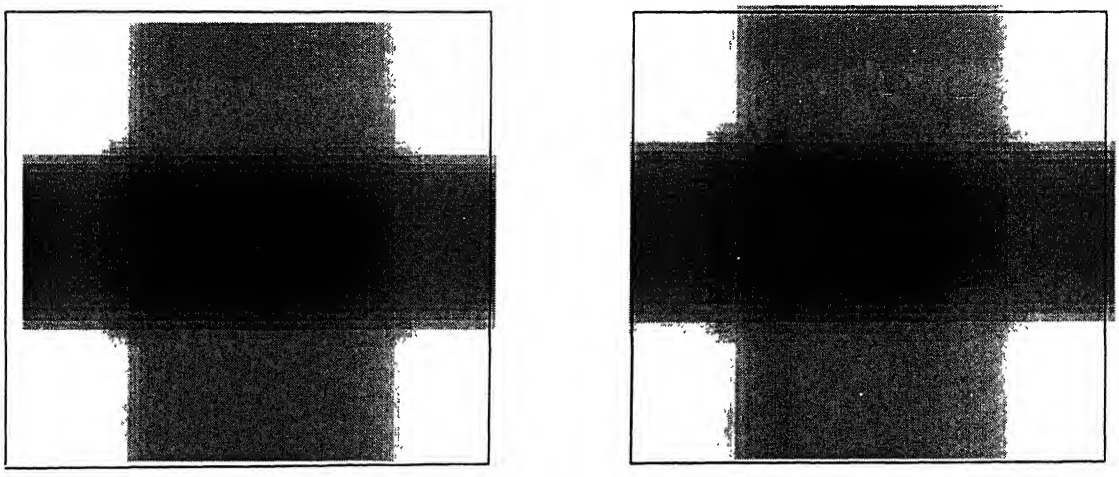

(a) $\lambda = 0.1$ (b) $\lambda = 1.0$

Fig. 5.7 (a-b) Tomographic reconstructed images from 2-view projection data for Elliptical Insertion with different relaxation parameters (λ) for Epoxy (faster material) inserted in the Perspex (slower material) sample with signal mode separation.

S. No.	Relaxation Parameter (λ)	Number of Iterations	Normalized RMS Error (EL2)
1	0.1	65	33.183
2	0.5	14	33.151
3	1.0	2	33.121
4	1.5	15	33.161

Table 5.7 Normalized RMS Error of the reconstructed images of the Epoxy elliptical inserted Nylon sample from 2-view projection data with different relaxation parameters (λ) with out signal mode separation.

Chapter 6

CONCLUSIONS AND SCOPE FOR FUTURE WORK

6.1 CONCLUSIONS

In the present work, ultrasonic tomographic reconstruction is used for reconstruction of domains of the samples with artificially implanted insertions. Based on the results obtained, the following conclusions are drawn:

- The wavelet transform is an excellent tool for noise suppression. A feature of this is that noise can be suppressed by utilization of different levels; where each level is depended upon the type of the signal.
- Correlation technique can be effectively employed for mode separation of the overlapped signal with any number of modes. This analysis results in accurate estimation of time of flight.
- A measure of energy-based criterion is proposed for selection of desired mode from the separated modes of an overlapped signal. This criterion is equally applicable for both fast and slow insertion medium.

6.2 SCOPE FOR THE FUTURE WORK

- These noise suppression and signal separation techniques can be extended to defect characterization in composite materials.
- More studies have to be made on wavelet analysis to apply it for mode separation in the overlapped signals.
- By the reconstruction of the images for 2-D slices of the defective sample, the reconstruction of 3-D defects can be carried out by integrating the 2-D slice images.

References

[1] Roy O., Sallard J., and Moubarik S. E. "Echo extraction from an ultrasonic signal using continuous wavelet transform", Review of Progressive in Quantitative Nondestructive Evaluation, Vol. 15, 1996, pp. 749-755.

[2] Agostino Abbate, Jeff Koay, Julius Frankel, Stephan C. Schroeder, and Pankaj Das. "Signal Detection and Noise Suppression Using a Wavelet Transform Signal Processor: Application to Ultrasonic Flaw Detection", IEEE Transactions on Ultrasonics, Ferroelectrics, and Frequency Control, Vol. 44, No. 1, January 1997, pp. 14-25.

[3] Guangming Zhang, Shuyi Zhang, and Yuwen Wang. "Application of Adaptive time-frequency decomposition in ultrasonic NDE of highly-scattering materials", Ultrasonics, Vol. 38, No. 10, November 2000, pp. 961-964.

[4] Guang-Ming Zhang, Ceng-Gang Hou, Yu-Wen Wang, and Shu-Yi Zhang. "Optimal frequency-to-bandwidth ratio of wavelet in ultrasonic non-destructive evaluation", Ultrasonics, Vol. 39, No. 1, January 2001, pp. 13-17.

[5] Castagnede B., Roux J., and Hosten B. " Correlation method for normal mode tracking in anisotropic media using an ultrasonic", Ultrasonic, Vol. 27, September 1989, pp. 280-287.

[6] Drai R., Sellidj F., Khelil M., and Benchaala A. "Elaboration of some signal processing algorithms in ultrasonic techniques: application to materials NDT", Ultrasonic, Vol. 38, 2000, pp. 503-507.

[7] Rolf K. Mueller, Mostafa Kaveh, and Glen Wade. "Reconstructive Tomography and Applications to Ultrasonic", Proceedings of The IEEE, Vol. 67, No. 4, April 1979, pp. 567-586.

[8] Avinash C. Kak. "Computerized Tomography with X-Ray, Emission, and Ultrasound Sources", Proceedings of IEEE, Vol. 67, No. 9, September 1979, pp. 1245-1279.

[9] Subbarao P. M. V., Munshi P., and Muralidhar K. "Performance of iterative Tomographic algorithms applied to non-destructive evaluation with limited data". NDT&E International, Vol. 30, No. 6, 1997, pp. 359-370.

[10] Krautkramer Josef, Krautkramer Herbert. "Ultrasonic Testing of Materials", Springer-Verlag Berlin Heidelberg, New York, 1983.

[11] Kishore N.N. and Datta D.. "Features of ultrasonic wave propagation to identify defects in composite materials modelled by finite element method", NDT&E International, Vol. 29, No. 4, 1996, pp. 213-223.

[12] Palanichamy P., Joseph A., Jayakumar T., and Baldev Raj. "Ultrasonic velocity measurements for estimation of grain size in austenitic stainless steel", ", NDT&E International, Vol. 28, No. 3, 1995, pp. 179-185.

[13] Chui C.K. "An introduction to Wavelets", Vol. 1, Academic press, Boston, 1992.

[14] Legendre S., Goyette J., and Massicotte D. "Ultrasonic NDE of composite material structures using wavelet coefficients", NDT&E International, Vol. 34, No. 1, January 2001, pp. 31-37.

[15] Cavaccini G., Agresti M., Borzacchiello, Bozzi E., Chimenti M., and Salvetti O. "An Evaluation Approach to NDT Ultrasound Processes by Wavelet Transform", Downloaded from http://www.ndt net.

[16] Beauchamp K. G. "Signal Processing, Using Analog and digital Techniques", London. George Allen & Unwin Ltd., 1973.

[17] Xiaoming Lai, Hans Torp, and Kjell Kristoffersen. "An Extended Autocorrelation Method Estimation of Blood Velocity", IEEE Transactions on Ultrasonics, Ferroelectrics, and Frequency Control, Vol. 44, No. 6, November 1997, pp. 1332-1342.

[18] Ignacio C. E., Charis L. de Korte, and Antonius F. W. van der Steen. " Echo Decorrelation from Displacement Gradients in Elasticity and Velocity Estimation", IEEE Transactions on Ultrasonics, Ferroelectrics, and Frequency control, Vol. 46, No. 4, July 1999, pp. 791-801.

[19] Ehreberg J. E., Ewart T. E. and Morris R. D. "Signal processing techniques for resolving individual pulses in a multipath signal", J. Acoustical Society of America, 1978, vol. 63, No 6, pp. 1861-1865.

[20] Dean Verhoeven. "Multiplicative algebraic computerized Tomographic algorithms for reconstruction of multidirectional interferometric data", Optical Engineering, Vol. 32, No. 2, February 1993, pp. 410-419.

[21] Yair Censor. "Finite Series-Expansion Reconstruction Methods", Proceedings of the IEEE, Vol. 71, No. 3, April 1983, pp. 409-419.

[22] Debasish Mishra, Muralidhar K., and Munshi P. " A Robust Mart Algorithm for Tomographic Applications", Department of Nuclear and Mechanical Engineering, Indian Institute of Technology-Kanpur.

[23] Datta, Debasis. "A Methodology in Ultrasonic NDE for Identification and Reconstruction of defects in Fiber Composites", Ph.D. Thesis, September 1995, Department of Mechanical Engineering, Indian Institute of Technology-Kanpur.

[24] Vijay Shankar Babu Ch. "Application of Wavelet Transform to crack detection in Ultrasonic NDE: an FEM Study", M. Tech. Thesis, March 2000, Department of Mechanical Engineering, Indian Institute of Technology-Kanpur.

[25] Pranav Kumar Varshney. "Experimental Gamma-rays Tomography with limited data", M. Tech. Thesis, Nuclear Engineering and Technology Programme, Indian Institute of Technology-Kanpur.

[26] Shekar Y. Mahajan, "Development of an automated ultrasonic C-scan system for composite materials", M.Tech. Thesis, 1989, Indian Institute of Technology-Kanpur.

[27] Venkatesh, C. V. "An Ultrasonic C-scan System to identify Damages in Impacted Fiber-Composite Plates", M. Tech. Thesis, January 1994, Department of Mechanical Engineering, Indian Institute of Technology-Kanpur.

PROGRAM FOR NOISE SUPPRESSION

Wavelet toolbox is a collection of functions on the MATLAB technical computing environment. It has been used for noise suppression of a given signal using 'db5' wavelet. The program used for the present work is given below.

```
% MATLAB PROGRAM FOR WAVELET DECOMPOSITION FOR NOISE
% SUPPRESION OF A SIGNAL WHICH IS USED IN THE PRESENT WORK

   wname='db5';      % Name of the wavelet which is using
   NUM=4;            % Number of the signal for decompose

% Reading the data from a file
   format short e;
   fid=fopen('FILENAME.m','r');
   n=fscanf(fid,'%d',[1.1]);
   AA=zeros(n,512);B=zeros(1,512);
   for i=1:n
      [B,count]=fscanf(fid,'%d',[1,512]);
     AA([i],:)=AA([i],:)+B;
   end
   status=fclose('all');
  AA;
  A=AA([NUM],:);
  plot(A);
  pause

% Wavelet decomposition using 'db3' wavelet 3-level decomposition
   [C,L]=wavedec(A,3,wname);      % Multi(3)-level 1-D wavelet decomposition
   cA3=appcoef(C,L,wname,3); % cA3-Extract 1-D Approximation coefficients
   cD3=detcoef(C,L,3);       % cD3-Extracts the Detail coefficients at level 3
   cD2=detcoef(C,L,2);       % cD2-Extracts the Detail coefficients at level 2
   cD1=detcoef(C,L,1);       % cD1-Extracts the Detail coefficients at level 1

% Reconstruct from Approximation coefficients-cA3
   A3=wrcoef('a',C,L,wname,3);

% Reconstruct from Detail coefficients-cD3
   D3=wrcoef('d',C,L,wname,3);

% Reconstruct from Detail coefficients-cD2
   D2=wrcoef('d',C,L,wname,2);
```

```
% Reconstruct from Detail coefficients-cD1
  D1=wrcoef('d',C,L,wname,1);

% Plotting the signal Approximation and details
  subplot(5,1,1);plot(A);gtext('Original Signal S')
  subplot(5,1,2);plot(A3);gtext('Approximation A3');
  subplot(5,1,3);plot(D3);gtext('Detail D3')
  subplot(5,1,4);plot(D2);gtext('Detail D2')
  subplot(5,1,5);plot(D1);gtext('Detail D1')

% In this program 'A3' is the Signal after suppress the noise
```

PROGRAM FOR SIGNAL SEPARATION USING LEAST-SQUARES METHOD

In this program Least squares method used for separating overlapped signal in to two modes, when two-reference signal are exist. MATLAB environment has been used in the present work. The program is given below.

```
% ********************************************************************
%    PROGRAM FOR SEPARATION OF THE OVERLAPPED SIGNAL USING
%    LEAST-SQUARES METHOD
% ********************************************************************
   wname='db5';  % Name of the wavelet (i.e. using)
   fwavno=1; % First Reference signal index
   owavno=2; % Overlapped signal index (from input file)
   lwavno=3; % Second reference signal

% Reading the data from a file
   format short e;
   fid=fopen('inputfile.m','r');
   n=fscanf(fid,'%d',[1.1]);
   DATA=zeros(n,512);B=zeros(1,512);

   for i=1:n
      [B,count]=fscanf(fid,'%d',[1,512]);
      DATA([i],:)=DATA([i],:)+B;
   end
   status=fclose('all');
   DATA;

% Shifting the axis of the signal to the x-axis
   A=zeros(n,512);
   for i=1:n
      A([i],:)=DATA([i],:)-round(mean(DATA([i],:)));
   end


% Least squares method starts
   FT=A([owavno],:);F1=A([fwavno],:);F2=A([lwavno],:);

   F11=sum(F1.*F1);F12=sum(F1.*F2);F13=sum(F1);
   F22=sum(F2.*F2);F23=sum(F2);F33=512;
   G1=sum(FT.*F1);G2=sum(FT.*F2);G3=sum(FT);
```

```
F=[F11 F12 F13;F12 F22 F23;F13 F23 F33]


G=[G1;G2;G3]
AA=F\G
a=AA([1]);b=AA([2]);c=AA([3]);
wav1=a*F1; wav2=b*F2;
twav=wav1+wav2+c;

% Plotting the signals
subplot(5,1,1);plot(FT);gtext('Overlapped Signal')
subplot(5,1,2);plot(F1);gtext('First Reference Signal')
subplot(5,1,3);plot(F2);gtext('Second Reference Signal')
subplot(5,1,4);plot(wav1);gtext('First separated Signal')
subplot(5,1,5);plot(wav2);gtext('Second separated Signal')

% Finding the error of summation (of the separated) signal
twav=wav1+wav2;
e=0;T=0;
for i=1:512
   a1=FT([i]);b1=twav([i]);
   e=e+abs((a1-b1)/b1);
end
e

pause
x=1:512;plot(x,twav,x,FT);
```

PROGRAM FOR SIGNAL SEPARATION USING CROSS CORRELATION METHOD

In this program Cross-correlation method used for separating overlapped signal in to two modes, when only one reference signal is exists. MATLAB environment has been used in the present work. The program is given below.

```
% ********************************************************************
%    PROGRAM FOR SEPARATION OF THE OVERLAPPED SIGNAL USING
%    CROSS CORRELATION METHOD
% ********************************************************************
   wname='db5';              % Name of the wavelet (i.e. using)
   fwavno=1;                 % Reference signal index (in the input file)
   owavno=2;                 % Overlapped signal index

% Reading the data from a file
   format short e;
   fid=fopen('inputfile.m','r');
   n=fscanf(fid,'%d',[1.1]);
   DATA=zeros(n,512);B=zeros(1,512);
   for v=1:n
       [B,count]=fscanf(fid,'%d',[1,512]);
       DATA([v],:)=DATA([v],:)+B;
   end
   status=fclose('all');

% Suppression noise of the signal
   DATA1=zeros(2,512);  A3=zeros(2,512);
   DATA1=DATA([fwavno],:);  DATA1=DATA([owavno],:);

   for i=1:2
      [C,L]=wavedec(DATA1([i],:),3,wname);

      cA3=appcoef(C,L,wname,3);
      cD3=detcoef(C,L,3);
      cD2=detcoef(C,L,2);
      cD1=detcoef(C,L,1);
      A3([i],:)=wrcoef('a',C,L,wname,3);
      D3=wrcoef('d',C,L,wname,3);
      D2=wrcoef('d',C,L,wname,2);
      D1=wrcoef('d',C,L,wname,1);
   end
% Cross correlation program Starts from here
```

```
RT=A3([1],:);ST=A3([2],:);
S=fft(ST,512);              % FFT of the Overlapped signal
R=fft(RT,512);              % FFT of the Reference signa
n=length(R);                % size of the array
RNU=R;SNU=S;
nyquest=1/2;
NU=(0:n-1)/(n/2)*nyquest;          % Frequency scale

N=2;                               % N -> Number of Modes
A=zeros(N,1);TAU=zeros(N,1);
for k=1:N                          % k -> For k modes, k = 1 to N
    for p=k:-1:1                   %  p -> For on Order p mode, p = k to 1
        TEMP=0+j*0;
        for g=1:N
            if g ~= p
               TEMP=TEMP+A(g)*exp(-2*j*pi*TAU(g)*NU);
            end
        end
        SP=SNU-RNU.*TEMP;
        ASP=abs(SP);
        RNU_R=RNU(512:-1:1);
        [MAX,pos] = max(abs(ifft(SP .* RNU_R)));
        TAU(p)=pos;
        ARNU=abs(RNU);
        A(p)=sum(ASP.^2)/sum(ARNU.^2); A(p)=sqrt(A(p))
    end
end
A,TAU

% Finding separated signal(in frequency mode) from amplitudes & time shifts
SP1=RNU.*(A(1)*exp(-2*j*pi*TAU(1)*NU));
SP2=RNU.*(A(2)*exp(-2*j*pi*TAU(2)*NU));

subplot(4,1,1);plot((ST),'k');grid on;gtext('Overlapped Signal S');
subplot(4,1,2);plot((RT),'k');grid on;gtext('Reference Signal R');

% Changing from frequency-domain to time-domain
SPT1=ifft(SP1);SPT2=ifft(SP2);

subplot(4,1,3);plot(real(SPT1),'k');grid on;gtext('First Separated Signal S_1');
subplot(4,1,4);plot(real(SPT2),'k');grid on;gtext('Second Separated Signal S_2');

% Addition of of two modes of the signal
SPT12=SPT1+SPT2;
Pause; subplot(1,1,1);plot(real(SPT12))
```